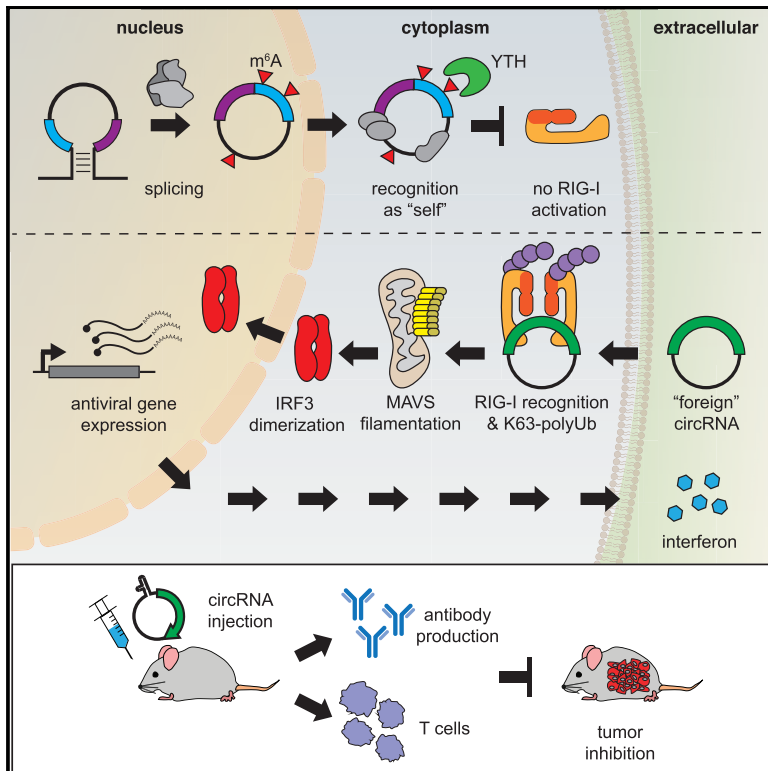# N6-Methyladenosine Modification Controls Circular RNA Immunity

Graphical Abstract

Authors

Y. Grace Chen, Robert Chen,
Sadeem Ahmad, ..., Bali Pulendran,
Sun Hur, Howard Y. Chang

Correspondence

howchang@stanford.edu

In Brief

Mammalian cells distinguish between foreign and endogenous circular RNAs (circRNAs), but the molecular basis is unknown. Chen et al. identify N6-methyladenosine (m6A) RNA modification as a marker for "self." Unmodified circRNA, but not m6A-modified circRNA, activates RIG-I in the presence of K63-polyubiquitin to cause MAVS filamentation, IRF3 dimerization, and interferon production.

Highlights

- Unmodified circRNA adjuvant induces antigen-specific T and B cell responses

- m6A RNA modification marks self circRNAs and abrogates circRNA immunity

- Unmodified circRNA and K63-polyubiquitin activate RIG-I and innate immune signaling

- YTHDF2 binding of m6A-circRNA additionally suppresses circRNA immunity

*N*6-Methyladenosine Modification Controls Circular RNA Immunity

Y. Grace Chen,[1,2,9] Robert Chen,[1,9] Sadeem Ahmad,[3,4] Rohit Verma,[5] Sudhir Pai Kasturi,[6] Laura Amaya,[1] James P. Broughton,[1] Jeewon Kim,[7] Cristhian Cadena,[3,4] Bali Pulendran,[5] Sun Hur,[3,4] and Howard Y. Chang[1,8,10,*]

[1]Center for Personal Dynamic Regulomes, Stanford University, Stanford, CA 94305, USA
[2]Department of Immunobiology, Yale School of Medicine, New Haven, CT 06519, USA
[3]Department of Biological Chemistry and Molecular Pharmacology, Harvard Medical School, Boston, MA 02115, USA
[4]Program in Cellular and Molecular Medicine, Boston Children's Hospital, Boston, MA 02115, USA
[5]Institute for Immunity, Transplantation and Infection, Department of Pathology, Department of Microbiology and Immunology, Stanford University, Stanford, CA 94305, USA
[6]Emory Vaccine Center/Yerkes National Primate Research Center at Emory University, Atlanta, GA, USA
[7]Stanford Cancer Institute, Stanford University, Stanford, CA 94305, USA
[8]Howard Hughes Medical Institute, Stanford University, Stanford, CA 94305, USA
[9]These authors contributed equally
[10]Lead Contact
*Correspondence: howchang@stanford.edu
https://doi.org/10.1016/j.molcel.2019.07.016

SUMMARY

Circular RNAs (circRNAs) are prevalent in eukaryotic cells and viral genomes. Mammalian cells possess innate immunity to detect foreign circRNAs, but the molecular basis of self versus foreign identity in circRNA immunity is unknown. Here, we show that *N*6-methyladenosine (m6A) RNA modification on human circRNAs inhibits innate immunity. Foreign circRNAs are potent adjuvants to induce antigen-specific T cell activation, antibody production, and antitumor immunity *in vivo*, and m6A modification abrogates immune gene activation and adjuvant activity. m6A reader YTHDF2 sequesters m6A-circRNA and is essential for suppression of innate immunity. Unmodified circRNA, but not m6A-modified circRNA, directly activates RNA pattern recognition receptor RIG-I in the presence of lysine-63-linked polyubiquitin chain to cause filamentation of the adaptor protein MAVS and activation of the downstream transcription factor IRF3. CircRNA immunity has considerable parallel to prokaryotic DNA restriction modification system that transforms nucleic acid chemical modification into organismal innate immunity.
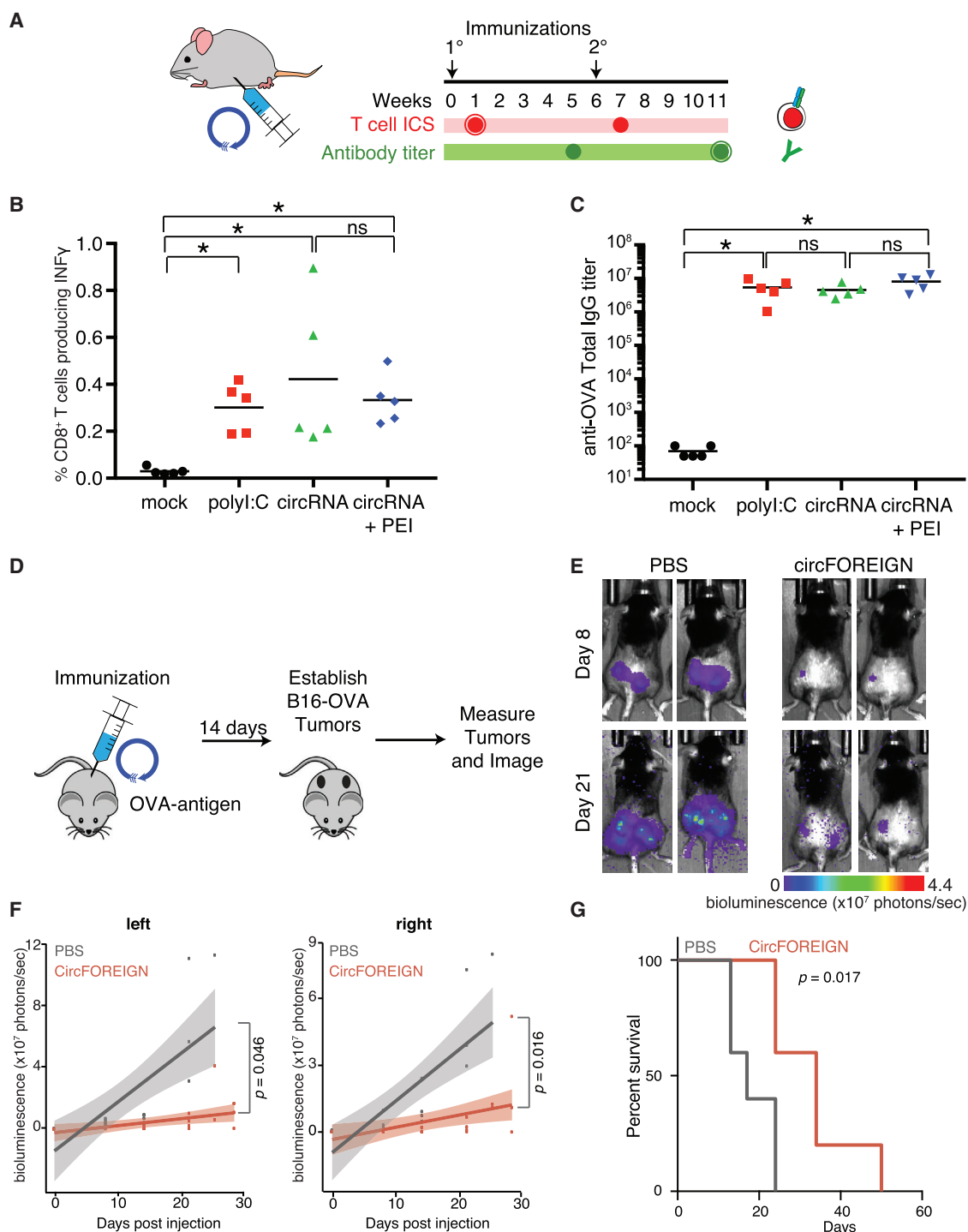
INTRODUCTION

Tens of thousands of circular RNAs (circRNAs) have been identified in eukaryotes (Hansen et al., 2013; Memczak et al., 2013). Viruses like the hepatitis delta virus and plant viroids possess circRNA genomes, and many viruses produce circRNAs in their replication cycle (Kos et al., 1986; Sanger et al., 1976; Toptan et al., 2018). Recent studies suggest an emerging picture of an innate immune system based on circRNAs. Introduction of certain exogenous circRNAs can activate an antiviral and immune gene expression program (Chen et al., 2017), while endogenous circRNAs can collectively inhibit protein kinase R and set the threshold for innate immunity upon virus infection (Liu et al., 2019). The mammalian innate immune system depends on pattern recognition receptors (PRRs) recognizing pathogen-associated molecular patterns (PAMPs) that are common among viruses and bacteria. RIG-I and MDA5 are PRRs found in the cytosol that sense foreign nucleic acids. MDA5 is known to detect long double-stranded RNA (dsRNA) whereas RIG-I has been characterized to recognize 5′ triphosphate on short dsRNAs (Hornung et al., 2006; Reikine et al., 2014). Although linear RNA ligands for RIG-I activation have been extensively characterized (Schlee and Hartmann, 2010), RIG-I interaction with circRNAs has not been investigated, especially in the context of foreign circRNA detection.

*N*6-methyladenosine (m6A) is one of the most abundant RNA modifications, present on 0.4%–0.6% of all cellular RNAs including mRNAs, long noncoding RNAs, and circRNAs (Dominissini et al., 2012; Meyer et al., 2012). On mRNAs, m6A has been demonstrated to regulate different functions including splicing (Xiao et al., 2016), translation (Meyer et al., 2015; Wang et al., 2015), and degradation (Wang et al., 2014), which have cell- and tissue-wide effects. Previous studies suggest that m6A is also present on circRNA and has the potential to initiate cap-independent translation (Legnini et al., 2017; Yang et al., 2017). However, the scope of m6A on circRNA function and the role in RIG-I detection of circRNAs are not known. m6A modification of 5′-triphosphate linear RNA ligands abrogates RIG-I binding and activation (Durbin et al., 2016; Peisley et al., 2013). However, these prior studies employed 100% m6A-modified short linear RNA ligands *in vitro*. Whether physiologic levels of RNA modification can be sensed by RIG-I, its relevance to other types of RNAs, nor its biological impact *in vivo* are not known.

Here, we investigate the role of m6A modification in innate immunity induced by exogenous circRNA. We evaluate circRNA immunogenicity *in vivo* and test the ability of circRNA induction

Figure 1. CircFOREIGN Induces Immune Response *In Vivo*

(A) Agonist RNA in conjunction with OVA is delivered by subcutaneous injection. T cell ICS and antibody titers are measured at the indicated times following primary and secondary immunizations.

(B) CircRNA stimulates anti-OVA T cell responses independent of transfection agent following primary vaccination. Means are shown (n = 5), *$p < 0.05$, Kruskal-Wallis test.

(C) CircRNA stimulates anti-OVA antibody titers independent of transfection agent following secondary vaccination. Means are shown (n = 5), *$p < 0.05$, ANOVA-Tukey's test.

of innate immunity to cross prime adaptive immunity in the contexts of vaccination and tumor immunity. We identify the m6A reader YTHDF2 on endogenous human circRNA and dissect the functional roles of YTHDF2 and RIG-I as the pattern recognition receptor for self versus foreign circRNAs.

RESULTS

In Vitro Production and Characterization of Immunogenic circRNA

A circularized GFP mRNA via permuted *td* intron from T4 bacteriophage, termed "circFOREIGN" hereafter, is highly immunogenic in cultured mammalian cells (Chen et al., 2017). *td* introns program autocatalytic splicing during *in vitro* transcription to form circFOREIGN. Prolonged treatment (>2 h) of circFOREIGN with exonuclease RNase R degraded linear RNA byproducts and yielded enriched circRNAs (Chen et al., 2017; STAR Methods). Subsequent alkaline phosphatase treatment removes 5′ phosphate from free ends. Delivery of foreign circRNAs into mammalian cells potently stimulated immune gene expression and protected against subsequent viral infection (Chen et al., 2017). A recent report suggests that exogenous circRNAs are not immunostimulatory, but rather 5′ triphosphorylated linear RNA contaminants due to incomplete RNase R digestion trigger immune response (Wesselhoeft et al., 2019). Wesselhoeft et al. (2019) used a short (30 min) RNase R treatment, no phosphatase treatment, and then performed high performance liquid chromatography (HPLC) to remove linear 5′ phosphorylated RNAs from circRNA. We have previously shown the immune stimulation by circFOREIGN synthesized *in vitro* and treated with phosphatase followed by RNase R for 2 h is comparable to the circFOREIGN treated with a second round of phosphatase to remove triphosphates on contaminating linear RNA, whereas linear RNA with phosphatase treatment has greatly reduced immune activation (Chen et al., 2017). This demonstrates that the circFOREIGN stimulation is independent of the presence of aberrant 5′ triphosphates in the sample. However, to confirm that 5′ triphosphates are not stimulating immune gene expression, we treat all circFOREIGN synthesized with phosphatase in this report.

We probed if gel purification of the circFOREIGN treated with RNase R altered the circFOREIGN immune stimulation. We reasoned that if there are contaminating linear RNA components that are contributing to the circFOREIGN's immunogenicity, then gel extraction would eliminate these contaminants, which have different molecular weights. The nicked-circRNA products in the gel are not immunostimulatory, because they become linear. We compared gel-purified circFOREIGN treated with RNase R and alkaline phosphate versus the same circFOREIGN preparation that underwent gel purification. Each RNA preparation was

transfected into HeLa cells, followed by qRT-PCR analysis of innate immunity genes 24 h later. The gel-purified circFOREIGN stimulated innate immune genes with similar potency compared to a standard preparation of circFOREIGN (Figures S1A and S1B).

We also subjected the synthesized circRNA treated with RNase R to HPLC fractionation. Size exclusion chromatography resolved the RNase-R-treated circRNA into two fractions (Figure S1C). Concentration and TapeStation analysis of each fraction reflected that the HPLC peak 1 and 2 mirror the results from gel electrophoresis of RNase R-treated circFOREIGN (Figure S1C). We noted that our HPLC purification chromatogram and resulting fractions differ from previously reported separation (Wesselhoeft et al., 2019) due to differences in instrumentation. Transfection of each fraction into HeLa cells followed by qRT-PCR revealed that the fraction with circRNA retained immune response (Figure S1D). Although peak 1 includes smaller degraded RNA and un-digested introns, this fraction was still immunogenic. This result is consistent with the interpretation that phosphatase treatment throughout the sample preparation had inactivated immunogenic linear RNAs. We found that circFOREIGN integrity was better-preserved in gel purification over HPLC purification with less degradation into smaller RNA fragments in the former, which correlates with better preservation of circFOREIGN immunogenicity.

We concluded that smaller linear RNA resulting from incomplete RNase R digestion was not responsible for circRNA immunogenicity in our preparation. Differences in circRNA sequence and cell types tested may also contribute to apparent different findings from Wesselhoeft et al. (2019) (more below). We found that our enzymatic purification process appeared to preserve circFOREIGN integrity the best, and thus continued with our enzymatic purification process circFOREIGN subjected to RNase R enrichment and phosphatase treatment.

CircFOREIGN Acts as Vaccine Adjuvant *In Vivo*

CircFOREIGN has previously been shown to potently stimulate immune gene expression (Chen et al., 2017), but its behavior *in vivo* is not known. We reasoned that circFOREIGN has the potential to activate innate immunity and thus act as a vaccine adjuvant to increase the efficacy of the vaccine. CircFOREIGN was *in vitro* transcribed, purified, and delivered in combination with chick ovalbumin (OVA) into C57BL/6J mice by subcutaneous injection. PolyI:C served as a positive control for RNA adjuvant. CircFOREIGN was delivered as naked RNA or after packaging in a transfection agent, polyethylenimine (PEI). We collected T cells and performed intracellular cytokine staining (ICS) 7 days following primary or secondary vaccinations and collected serum and measured antibody responses 5 weeks after vaccinations (Figure 1A). Induction of OVA-specific,

(D) CircFOREIGN vaccination in conjunction with OVA is delivered by subcutaneous injection. 14 days later, OVA-expressing B16-melanoma cells are established in right and left flanks. Tumors are measured and imaged.

(E) CircFOREIGN vaccination decreases the rate of tumor growth. Representative images of bioluminescence of left and right tumors for mice vaccinated with PBS or circFOREIGN prior to tumor establishment.

(F) Quantification of bioluminescence measurements in left and right tumors for mice vaccinated with PBS or circFOREIGN prior to tumor establishment. *p* value calculated by Wilcoxon signed-rank test. n = 5 mice in each group.

(G) Mice vaccinated with circFOREIGN survive twice as long as negative control mice. Survival curves for mice vaccinated with PBS or circFOREIGN prior to tumor establishment. *p* value calculated by log-rank test. n = 5 mice in each group.

interferon gamma-positive (Ifnγ[+]) activated CD8 T cells required adjuvant such as polyI:C, as expected (Figures 1B and S2A–S2C). Notably, co-injection of circFOREIGN induced potent anti-OVA T cell to comparable levels as polyI:C, either with naked circRNA ($p = 0.0088$ compared to mock, ANOVA-Tukey's test) or in PEI nanoparticles ($p = 0.0039$ compared to mock, ANOVA-Tukey's test, Figure 1B). Measurement of OVA-specific antibodies revealed that circFOREIGN alone stimulates antibody production to comparable levels as the positive control polyI:C (Figures 1C and S2B). CircFOREIGN did not require a transfection reagent in order for stimulation of OVA-specific CD8^{+} T cells and antibodies. In fact, the CD8^{+} T cell responses were higher in injections without PEI, and we omitted PEI in subsequent experiments.

After immunization of mice with circFOREIGN or control, we isolated dendritic cells (DCs) from draining lymph nodes. We found that circFOREIGN adjuvant activated both cDC1 and cDC2 subsets, as judged by increased cell surface expression of the costimulatory molecule CD86 over control (Figures S2D and S2E). These results provide direct evidence *in vivo* that circRNA inoculation activated DCs. DC activation can, in principle, facilitate antigen cross presentation and activation of CD4^{+} Tfh cells and CD8^{+} T cells. However, circRNA may also directly affect T cells and other immune cell types, which remain to be explored.

CircFOREIGN Can Induce Anti-tumor Immunity

Because the delivery of circFOREIGN induces CD8^{+} T cell responses, we hypothesized that mice that were exposed to circFOREIGN and OVA would have adaptive immunity against OVA-expressing tumors. Thus, we vaccinated mice with circFOREIGN and OVA and 2 weeks later, implanted OVA-expressing B16 melanoma cells into the right and left flanks of the mice (Figure 1D). The OVA-B16 melanoma model is immune restricted largely through CD8^{+} effector T cells (Budhu et al., 2010). Mice receiving circFOREIGN have lower tumor growth compared to negative control mice receiving PBS (Figures 1E, 1F, and S2F). The left and right tumors in each mouse are correlated with each other, demonstrating that there is a systemic-wide effect from the vaccination. The mice that were vaccinated with circFOREIGN just once have nearly doubled overall survival compared to the negative control mice ($p = 0.0173$, log-rank test, Figure 1G) and were comparable to the mice receiving positive control polyI:C HMW (Figure S2G). These results indicate that circRNA immunity can be harnessed toward potential therapeutic ends.

Endogenous circRNA Associate with m[6]A Machinery

Given that mammalian cells have endogenous circRNAs, their immune response to circFOREIGN suggests that they distinguish between self and non-self circRNAs. CircRNAs are produced through back-splicing to covalently join the 3′ and 5′ ends of RNA exons. Because intron identity dictates circRNA immunity (Chen et al., 2017) but is not part of the final circRNA product, we reasoned that introns may direct the deposition of one or more covalent chemical marks onto the circRNA. Among the over 100 known RNA chemical modifications, m[6]A is the most abundant modification on linear mRNAs and long noncod-
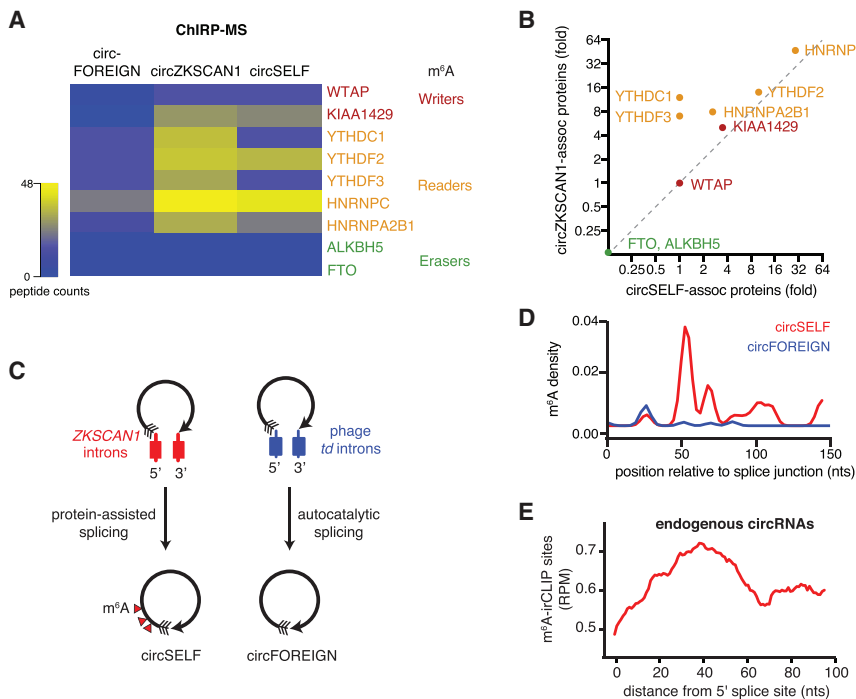
ing RNAs, and is present on 0.4%–0.6% of all adenosines in mammalian polyA-tailed transcripts (Roundtree et al., 2017). m[6]A has recently been detected on mammalian circRNAs (Zhou et al., 2017).

CircZKSCAN1 is a human circRNA produced by its endogenous introns and not immunogenic when expressed in human cells. We used the *ZKSCAN1* introns to program the production of circGFP, termed "circSELF." We transfected DNA plasmids encoding circRNAs generated by protein-assisted (circSELF) or autocatalytic splicing (circFOREIGN) into HeLa cells and performed comprehensive identification of RNA binding proteins by mass spectrometry (ChIRP-MS) experiments (Chen et al., 2017). We analyzed writers, readers, and erasers of covalent m[6]A modification (Roundtree et al., 2017) in association with circRNAs (Figure 2A). We found that *circZKSCAN1*, but not circFOREIGN, is associated with components of the m[6]A writer complex, such as WTAP and KIAA1429 (also known as Virilizer homolog or VIRMA) as well as the m[6]A reader proteins YTHDF2, HNRNPC, and HNRNPA2B1 (Figure 2A). Neither circRNA is associated with putative m[6]A demethylases ("erasers"), such as FTO and ALKBH5. Importantly, circSELF is the same circRNA sequence as circFOREIGN, but is no longer immunogenic (Chen et al., 2017), and is now associated with m[6]A writer and reader proteins (Figure 2A). Two different circRNAs (circSELF and *circZKSCAN1*) programmed by human introns achieve similar levels of association with m[6]A writer and reader proteins, including WTAP, KIAA1429, and YTHDF2 (Figure 2B). These results suggest that m[6]A modification machinery is transferred to exonic circRNAs as a memory of the introns that mediate their biogenesis, which occurs independently of circRNA sequence.

Self and Foreign circRNAs Have Different m[6]A Modification Patterns

We next defined the m[6]A modification patterns of human and foreign circRNAs. In human cells programmed to express the appropriate circRNAs, we used RNase R treatment to enrich for circRNAs and then performed m[6]A-UV-C crosslinking and m[6]A immunoprecipitation (m[6]A-irCLIP) (Zarnegar et al., 2016) to map the sites of m[6]A modification with high sensitivity (Figure 2C). m[6]A-irCLIP of circSELF versus circFOREIGN revealed that circSELF gained m[6]A modification within 50–100 nucleotides (nt) at the 3′ side of the circularization junction (Figure 2D). We did not observe other significant differences in modification through the rest of the transcript (Figure S3A). Because circSELF and circFOREIGN are the same exonic sequence circularized by a human (self) or phage (foreign) intron, this result indicates that human introns are sufficient to place m[6]A modification on the resulting circRNA. Moreover, comparison of endogenous circRNAs subjected to m[6]A-irCLIP to model human-programmed circRNA indicates that both have similar patterns of m[6]A modification (Figure 2E). m[6]A is enriched in the +40–100 nt window 3′ of the back-splice junction on endogenous circRNAs transcriptome-wide (Figure 2E). m[6]A is known to be enriched at the last exon of linear mRNA and lncRNAs (Figure S3B) (Dominissini et al., 2012; Ke et al., 2015; Meyer et al., 2012). Our finding of m[6]A modification 3′ of the back-splice junction is consistent with this pattern. Splicing occurs co-transcriptionally from 5′ to 3′, and the 3′ to 5′ back

Figure 2. CircSELF but Not CircFOREIGN Associate with m⁶A Machinery and Are Modified by m⁶A

(A) Heatmap of peptide counts from ChIRP-MS of circZKSCAN1, circSELF, and circFOREIGN. Enzymes are classified as m^{6}A writers, readers, and erasers.

(B) m^{6}A machinery associates with circZKSCAN1 and circSELF but not circFOREIGN, as indicated by ChIRP-MS. Fold enrichment over RNase-treated control is shown.

(C) Model showing ZKSCAN1 introns directing protein-assisted splicing to yield m^{6}A-modified circSELF and phage *td* introns directing autocatalytic splicing to form unmodified circFOREIGN.

(D) m^{6}A-irCLIP identifies high-confidence m^{6}A positions proximal to circRNA splice junction. *ZKSCAN1* introns suffice to direct m^{6}A modification on circSELF (red) compared with td intron-directed circFOREIGN (blue). Density of m^{6}A-irCLIP reads normalized to reads per million.

(E) m^{6}A-irCLIP read density near circRNA splice junction of endogenous human circRNAs in HeLa cells. Density of m^{6}A-irCLIP reads normalized to reads per million for reads proximal to circRNA splice junctions.

splice expected is the last splicing event on a circRNA (i.e., no intron remains to be spliced out).

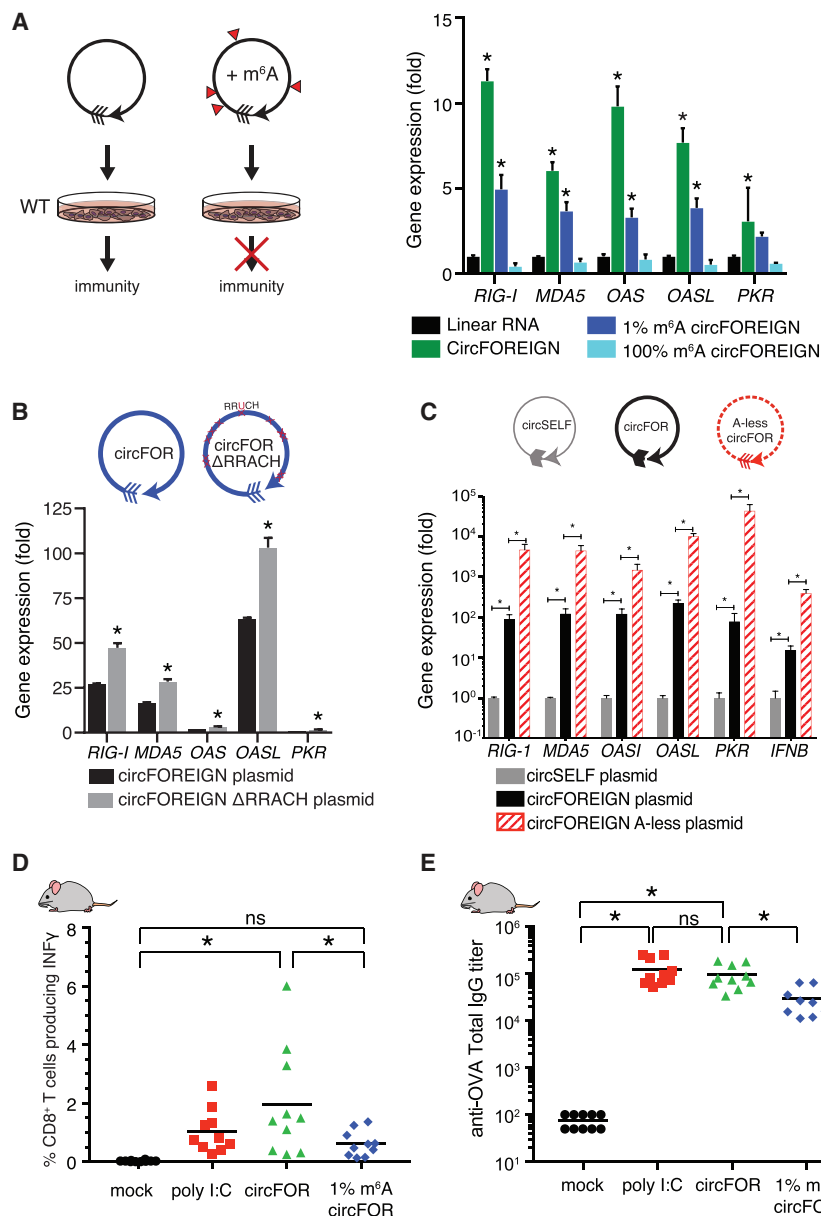## m⁶A Modification Marks circRNA as "Self"

We hypothesized that the chemical modification itself or in combination with the recognition of the m^{6}A by RNA-binding proteins allows marking of "self" circRNA. First, we tested whether incorporation of m^{6}A into circFOREIGN would mask the "non-self" identity and decrease the immunogenicity of the circFOREIGN. We synthesized unmodified or m^{6}A-modified circFOREIGN by *in vitro* transcription (Chen et al., 2017) and purified the circRNA by RNase R and phosphatase treatment. Incorporation of m^{6}A modification into circRNA does not affect splicing to form circRNA, while RNase R treatment enriches for m^{6}A-modified circRNA (Figures S3C and S3D). We then transfected the circFOREIGN into recipient cells and measured anti-viral gene expression. We note that circRNA m^{6}A modification in cells is concentrated at specific positions along the transcript, whereas m^{6}A incorporation during *in vitro* transcription is random. Thus, we chose to replace all adenosines with m^{6}A (100% m^{6}A) or add in just 1% m^{6}A into the circRNA to yield an average of 3 m^{6}A modifications for each circRNA. We reasoned that 100% m^{6}A is supra-physiologic but models the consecutive occurrence of m^{6}A observed *in vivo*. 1% m^{6}A models the overall level of m^{6}A ratio on endogenous RNA but not their modification pattern. CircFOREIGN potently induced a panel of antiviral genes, including *RIG-I*, *MDA5*, *OAS*, *OASL*, and *PKR*, and anti-viral gene induction was completely abrogated when all of the adenosines were replaced with m^{6}A modification (Figure 3A, 100% m6A). 1% m^{6}A incorporation significantly reduced but did not eliminate anti-viral gene induction (Figure 3A). Thus,

m^{6}A modification sufficed to reduce the immunogenicity of a foreign circRNA in cultured cells.

We then modified the circFOREIGN plasmid, eliminating m^{6}A consensus motifs (Dominissini et al., 2012) by mutating all instances (n = 12) of RRACH sequence to RRUCH in *GFP* exon. We hypothesized that when circFOREIGN is transcribed in the nucleus of human cells, METTL3/14 may modify circFOREIGN at low level, which would be abrogated in the ΔRRACH mutant. We transfected plasmids encoding wild-type or mutant circRNA into HeLa cells and then quantified circRNA levels and innate immunity gene induction by qRT-PCR. The gene induction is then normalized to the level of the measured circRNA. We found that RRACH site mutation significantly increased circRNA induction of anti-viral genes by ∼2-fold (Figure 3B). Because m^{6}A is enriched on, but not exclusively present at, RRACH motif, we next constructed a modified circFOREIGN plasmid where all adenosines are mutated to uracil in the GFP exons (A-less circFOREIGN) (Figure 3C). Transfection of plasmids encoding the A-less circRNA led to ∼10,000-fold-increase in anti-viral gene induction over circFOREIGN. These results provide the first evidence that specific circRNA exonic sequences impact immunity and specifically suggest endogenous m^{6}A modification dampens innate immunity.

m⁶A Modification of circRNA Blunts Vaccination Response *In Vivo*

m^{6}A modification also decreased the immunogenicity of circRNA as adjuvant *in vivo*. When we used 1% m^{6}A-modified circFOREIGN in the same adjuvant regime as unmodified circFOREIGN, we found that 1% m^{6}A modification substantially reduced both the activated CD8 T cell response (Figure 3D versus Figure 1B) and antibody titers (Figure 3E versus

Figure 3. m6A-Modified CircFOREIGN Attenuates Immune Response *In Vitro* and *In Vivo*

(A) Left: Model of unmodified and m6A-modified circFOREIGN effects of immunogenicity. Right: Transfection of unmodified circFOREIGN into wild-type HeLa cells stimulates immune response, but m6A-modified circFOREIGN does not. Graph showing gene expression of innate immune genes 24 h following RNA transfection. Relative expression of the indicated mRNA and transfected RNA are measured by qRT-PCR, results normalized to expression following mock transfection. Means ± SEM are shown (n = 3), *$p < 0.05$, Student's t test, comparing gene stimulation of linear RNA to indicated RNA.

(B) Transfection of circFOREIGN plasmid lacking RRACH m6A consensus motifs stimulates immune response at a greater level than circFOREIGN. RRACH motifs (n = 12 sites) were mutated to RRUCH throughout the exon sequence. Graph showing gene expression of innate immune genes following DNA plasmid transfection. Relative expression of the indicated mRNA and transfected RNA are measured by qRT-PCR, results normalized to expression following mock transfection. Means ± SEM are shown (n = 3), *$p < 0.05$, Student's t test, comparing circFOREIGN to indicated RNA transfection.

(C) Transfection of circFOREIGN plasmid with all adenosines replaced by uracil results in elevated immunogenicity. Relative expression of the indicated mRNA and transfected RNA are measured by qRT-PCR, results normalized to expression following mock transfection. Means ± SEM are shown (n = 3), *$p < 0.05$, Student's t test, comparing circFOREIGN to indicated RNA transfection.

(D) m6A-modified circFOREIGN attenuates anti-OVA T cell responses following primary vaccination. Means are shown (n = 10), *$p < 0.05$, ANOVA-Tukey's test.

(E) m6A-modified circRNA attenuates anti-OVA antibody titers following secondary vaccination. Means are shown (n = 10), *$p < 0.05$, ANOVA-Tukey's test.
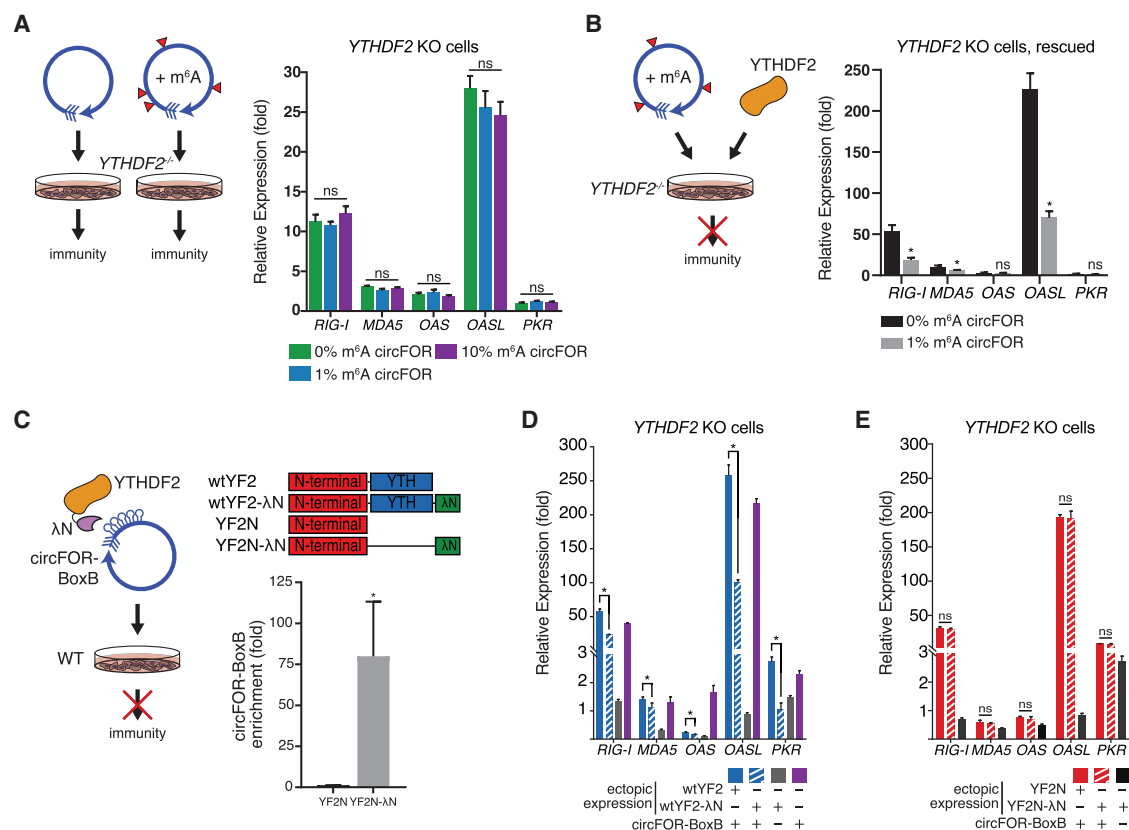
Figure 1C). We observed that repeated immunizations with 1% m6A-modified circFOREIGN induced an immune response that is diminished but not null (Figure S4). These results show that circFOREIGN is a potent immune stimulant *in vivo*, and 1% m6A modification is sufficient to blunt circRNA immunity.

YTHDF2 Reader Protein and Suppression of circRNA Immunity

We next sought to define the mechanisms of m6A suppression of circRNA immunity. m6A is recognized by a family of reader proteins, the most prominent of which are the YTH-domain containing RNA binding proteins (Dominissini et al., 2012; Edupuganti et al., 2017). We focused on YTHDF2 because (1) it is the main m6A reader we detected in association with endogenous circRNA or circSELF (Figures 2A and 2B), and (2) YTHDF2 is

cytoplasmic, the same compartment as endogenous and transfected circRNAs (Chen et al., 2017; Rybak-Wolf et al., 2015; Salzman et al., 2012). CircFOREIGN transfection into $YTHDF2^{-/-}$ HeLa cells (Figure S5A) led to potent induction of anti-viral genes (Figure 4A). Moreover, incorporation of 1% or 10% m6A into circFOREIGN no longer suppressed the antiviral gene induction in $YTHDF2^{-/-}$ cells (Figure 4A). An independent $YTHDF2^{-/-}$ clone gave very similar results (Figure S5B). Furthermore, ectopic expression of YTHDF2 in $YTHDF2^{-/-}$ cells rescued the suppression of immune gene induction in response to m6A-modified circFOREIGN (Figure 4B), indicating that YTHDF2 is required for mediating the "self" identity of m6A-marked circRNAs.

We next tested which domains of YTHDF2 are necessary for suppressing immune stimulation by circFOREIGN. We first

Figure 4. m⁶A-Modified CircFOREIGN Evades Non-self Detection through the Binding of YTHDF2

(A) YTHDF2 is necessary for differential response to unmodified versus m⁶A-modified circFOREIGN. Transfection of unmodified or m⁶A-modified circFOREIGN into *YTHDF2⁻/⁻* HeLa cells stimulate immune response. Left: Model showing the responses to unmodified or m⁶A-modified circFOREIGN. Right: Graph showing gene expression of innate immune genes 24 h following RNA transfection. Relative expression of the indicated mRNA and transfected RNA are measured by qRT-PCR, results normalized to expression following mock transfection. Means ± SEM are shown (n = 3). Student's t test, comparing circFOREIGN with 0% m⁶A to indicated RNA transfection.

(B) Ectopic expression of YTHDF2 rescues response to unmodified versus m⁶A-modified circFOREIGN in YTHDF2 KO HeLa cells. Left: Model showing response to m⁶A-modified circFOREIGN following rescue. Right: Graph showing gene expression of innate immune genes 24 h following RNA transfection. Relative expression of the indicated mRNA and transfected RNA are measured by qRT-PCR, results normalized to expression following mock transfection. Means ± SEM are shown (n = 3). *$p < 0.05$, Student's t test, comparing 0% m⁶A circFOREIGN to 1% m⁶A circFOREIGN.

(C) Tethering of YTHDF2 to unmodified circFOREIGN masks circRNA immunity. Left: Model showing *in* vivo tethering of protein to RNA via lambdaN and BoxB leading to attenuation of immunogenicity. Right top: Protein domain architecture of full-length wild-type YTHDF2 with and without lambdaN tethering tag, and YTHDF2 N-terminal domain with and without lambdaN tethering tag. Right bottom: RIP-qPCR enrichment of indicated YTH protein followed by qRT-PCR of circRNA-BoxB or control actin RNA. Means ± SEM are shown (n = 3). *$p < 0.05$, Student's t test, comparing YTHDF2 N terminus with lambdaN tethering to YTHDF2 N terminus without tethering.

(D) Transfection of unmodified circBoxB tethered to full-length wild-type YTHDF2 into wild-type HeLa cells attenuates immune response. Graph showing gene expression of innate immune genes 24 h following RNA transfection. Relative expression of the indicated mRNA and transfected RNA are measured by qRT-PCR, results normalized mock transfection. Wild-type YTHDF2-lambdaN (gray) was ectopically expressed as immunogenicity negative control. Transfection with solely circBoxB (purple) serves as immunogenicity positive control. Means ± SEM are shown (n = 3). *$p < 0.05$, Student's t test, comparing circBoxB with wild-type YTHDF2 with lambdaN tethering to wild-type YTHDF2 without tethering.

(E) Transfection of unmodified circBoxB tethered to N-terminal domain of YTHDF2 into YTHDF2 KO cells is insufficient to attenuate immune response. Graph showing gene expression of innate immune genes 24 h following RNA transfection. Relative expression of the indicated mRNA and transfected RNA are measured by qRT-PCR, results normalized mock transfection. N-terminal domain of YTHDF2-lambdaN (black) was ectopically expressed as immunogenicity negative control. Means ± SEM are shown (n = 3). Student's t test, comparing circBoxB with YTHDF2 N terminus with lambdaN tethering to YTHDF2 N terminus without tethering.

artificially tethered full-length YTHDF2 (Figure 4C) to unmodified circFOREIGN and tested whether the proximity of m⁶A reader proteins can bypass the need for m⁶A modification to suppress circRNA immunity. We introduced five consecutive BoxB stem loop RNA elements into circFOREIGN immediately after the splice junction, which we termed "circFOREIGN-BoxB"

(Baron-Benhamou et al., 2004). Additionally, we cloned C-terminal lambdaN peptide tags into proteins we tested and confirmed their expression via western blot (Figures S5C and S5D). The BoxB stem loops and lambdaN system enabled recruitment of YTH proteins fused to a lambdaN peptide to circFOREIGN-BoxB RNA, as confirmed by RIP-qPCR (Figures 4C and S5E).

Transfection of circFOREIGN-BoxB RNA alone strongly stimulated anti-viral genes, and tethering of full-length YTHDF2 significantly diminished antiviral gene induction (Figure 4D).

To evaluate if the N-terminal domain of YTHDF2, termed YTHDF2N, is sufficient for immune evasion of circFOREIGN, we tethered YTHDF2 N terminus to unmodified circFOREIGN-BoxB. The N terminus was not sufficient to suppress immune response to circFOREIGN-BoxB (Figure 4E). Because the N-terminal domain is responsible for cellular localization of YTHDF2-RNA complex, and the C-terminal domain selectively binds to m6A-modified RNA (Wang et al., 2014), the C-terminal domain is likely required for diminishing antiviral gene induction by circFOREIGN-BoxB.

We then probed if the YTH domain is capable of marking circFOREIGN-BoxB as self by joining YTH to unmodified circFOREIGN-BoxB (Figure S5F). There was no significant change in RIG-I gene expression between circFOREIGN alone and circFOREIGN tethered to the YTH domain. However, tethering circFOREIGN-BoxB and YTH significantly increased the expression of *MDA5* and *OAS1*. Because full-length YTHDF2 protein is larger than each of the separate domains, we probed if tethering circFOREIGN-BoxB to red fluorescent protein (RFP) would affect cellular recognition of unmodified circRNA (Figure S5G). There is a modest decrease in stimulation of *RIG-I* gene expression, but none of the other immune sensors tested changed expression. This suggests that full suppression of circFOREIGN-BoxB immunogenicity requires all of the YTHDF2 domains, and greater interaction between another protein and circRNA is not sufficient.

To test if other members of the YTH family are involved in immune suppression of circFOREIGN, we probed the effects of tethering YTHDF1, another cytoplasmic m6A reader protein to circFOREIGN-BoxB. Following transfection of DNA plasmids, the N terminus of YTHDF1 also failed to diminish antiviral gene induction, similar to YTHDF2 (Figure S5H). Taken together, these results demonstrate that the full-length m6A reader protein is necessary to mask circRNA immunity and circRNA requires either the m6A chemical modification or m6A reader protein to distinguish between "self" and "foreign" circRNAs.

m6A Writer METTL3 Needed for Self/Non-self Recognition of circRNA

To probe the necessity of m6A in conveying a "self" mark on the circRNAs, we investigated the role of METTL3, the catalytic subunit of the writer complex for installing the m6A modification. METTL3 is essential for embryonic development due to the critical role of m6A in timely RNA turnover (Batista et al., 2014). METTL3 depletion in many human cancer cell lines leads to cell death. We surmised that one possible consequence of METTL3 depletion is a deficit of m6A modification of endogenous circRNA, leading to immune activation. RIG-I is a RNA binding and signaling protein that senses viral RNA for immune gene activation (Wu and Hur, 2015). We previously showed that foreign circRNAs co-localize with RIG-I in human cells, and RIG-I is necessary and sufficient for circRNA immunity (Chen et al., 2017). Thus, if m6A is required to prevent cells from recognizing their own circRNA as foreign and initiating an immune response, then concomitant RIG-I inactivation should ameliorate

the response. Indeed, METTL3 depletion in wild-type HeLa cells led to widespread cell death, but *RIG-I* inactivation in HeLa (Chen et al., 2017) rescued the cell death (Figure S6). These results suggest that one function of m6A is to prevent RIG-I activation by self RNAs, although we cannot rule out indirect effects due to other RNA targets of METTL3.
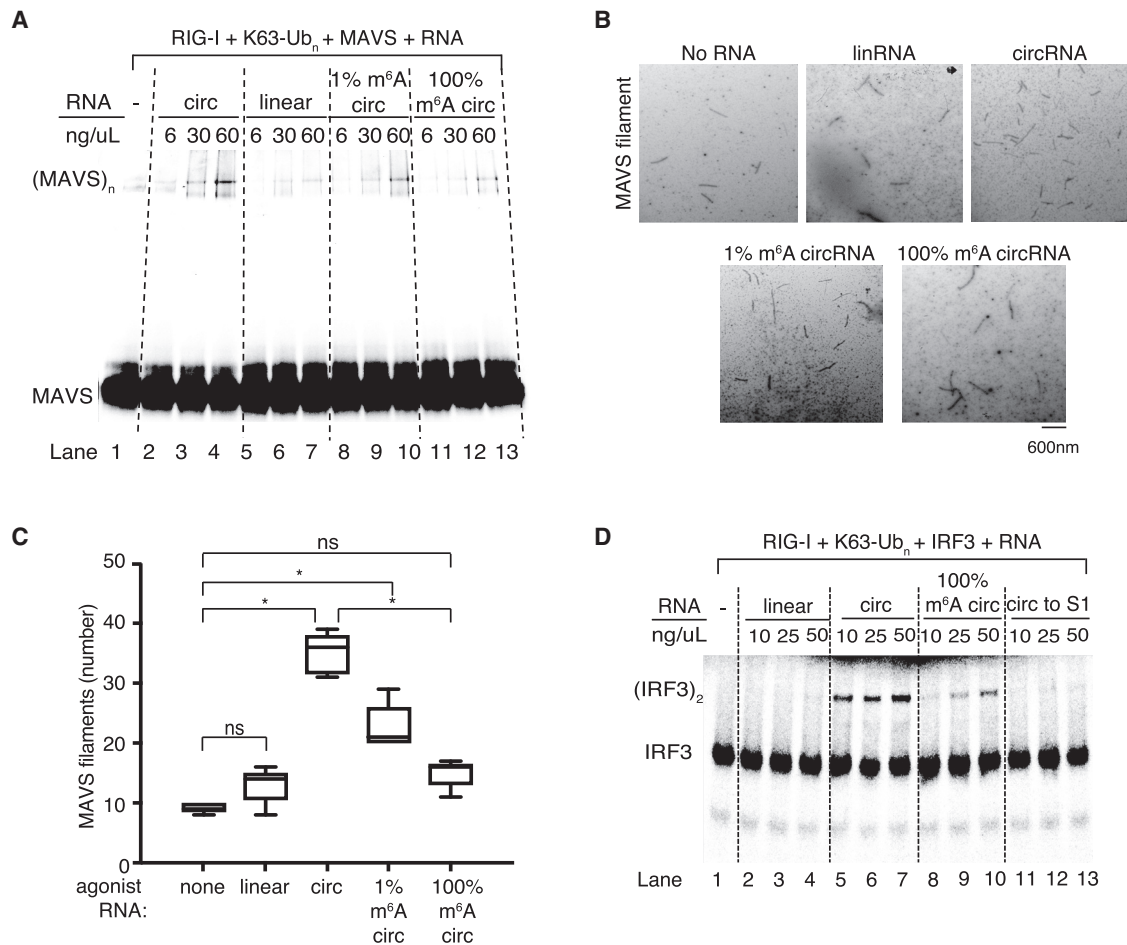
CircFOREIGN Recognition by RIG-I Is Distinct from Linear RNA Ligand

To probe the mechanism of how circRNA stimulates an innate immune response, we turned to biochemical reconstitution with purified components. First, we tested the ability of circFOREIGN to induce ATP hydrolysis by RIG-I. When RIG-I recognizes the 5′-triphosphate dsRNA agonist, the protein's helicase domain hydrolyzes ATP (Hornung et al., 2006; Schlee et al., 2009). Exposure of RIG-I to circFOREIGN or 5′ hydroxyl linear RNA did not stimulate its ATPase activity, whereas a 512-bp 5′-triphosphate dsRNA induced ATP hydrolysis by RIG-I (Figure S7A). Next, we tested for the ability of circFOREIGN to activate purified RIG-I by forming filaments directly on circFOREIGN. Electron microscopy imaging of RIG-I, circFOREIGN, and ATP did not reveal the obvious formation of filaments, whereas the positive control 5′-triphosphate dsRNA induced RIG-I polymerization (Figure S7B). Thus, circFOREIGN does not interact with nor activate RIG-I in the same manner as 5′-triphosphate RNA ligands, as expected.

CircFOREIGN Directly Binds RIG-I and K63-Polyubiquitin Chain

An alternate mechanism of RIG-I activation involves lysine 63 (K63)-linked polyubiquitin chains (K63-Ub_n), which interact with and stabilize RIG-I 2CARD domain oligomers (Jiang et al., 2012; Peisley et al., 2014; Zeng et al., 2010). We probed the ability of RIG-I to bind unmodified and m6A-modified circFOREIGN and the dependency of the interaction on K63-Ub_n chains. Using a native gel shift binding assay with purified RIG-I and circFOREIGN, we find that RIG-I binds positive control 5′-triphosphate 162 bp dsRNA both in the absence (Figure S7C, lane 2) and presence (Figure S7C, lanes 3 and 4) of K63-Ub_n. We find that RIG-I binds both unmodified and m6A-modified circFOREIGN (Figure S7C, lanes 5–16). Although K63-Ub_n chains do not seem to be necessary for RIG-I binding to circFOREIGN, there is greater binding of RIG-I to circFOREIGN when the concentrations of K63-Ub_n chains are high (Figure S7C, lane 7 versus lane 8, lane 11 versus lane 12, and lane 15 versus lane 16). Because RIG-I binds to both unmodified and m6A-modified circRNA but is activated only by the former (more below), these results suggest that RIG-I discriminates between unmodified and m6A-modified circRNA at the level of conformational change, rather than binding. These results further support that RIG-I binding to circRNA is different than 5′-triphosphate dsRNA ligands.

PRRs like RIG-I and MDA5 survey many RNAs, but only selectively undergo conformational change for oligomerization upon interaction with immunogenic RNA ligands (Ahmad et al., 2018). Similarly, the selectivity of RIG-I for 5′ triphosphate (present on viral RNAs) over m7G cap (present on all mRNAs) is due to conformational change rather than ligand binding (Devarkar et al., 2016). Therefore, we next examine whether RIG-I

A RIG-I + K63-Ub$_n$ + MAVS + RNA

B MAVS filament

No RNA · linRNA · circRNA

1% m^{6}A circRNA · 100% m^{6}A circRNA

600nm

C

D RIG-I + K63-Ub$_n$ + IRF3 + RNA

Figure 5. RIG-I Directly Distinguishes Unmodified versus m^{6}A-CircFOREIGN and Initiates Innate Immune Signaling Cascade
(A) *In vitro* reconstitution with purified RIG-I, MAVS, K63-Ub$_n$, and the indicated RNA ligands. Native gel of fluorescently labeled MAVS 2CARD domain is shown.
(B) Representative electron microscopy images of MAVS filaments after MAVS polymerization assay with indicated RNAs. Scale bar indicates 600 nm.
(C) Quantification of the total number of MAVS filaments observed in five electron microscopy images for each agonist RNA. *$p < 0.05$, Student's t test.
(D) *In vitro* reconstitution of the circRNA-mediated induction of IRF3 dimerization. Native gel of radiolabeled-IRF3 with the indicated RNA ligands is shown. S1 is cellular extract.

discriminates against m^{6}A-modified circRNA at the level of binding versus conformational change.

CircFOREIGN Sensing: RIG-I and K63-Polyubiquitin Chain Activate MAVS and Discriminates m^{6}A

When RIG-I is activated, oligomerized RIG-I templates the polymerization of mitochondrial anti-viral signaling protein (MAVS, also known as IPS-1, Cardif, and VISA) into filaments, creating a platform for subsequent signal transduction that culminates in the activation and dimerization of IRF3 transcription factor. We reconstituted purified circFOREIGN, RIG-I, K63-Ub$_n$, and MAVS *in vitro*, and we monitored MAVS transition from monomer into filament by gel shift (Figure 5A) or electron microscopy (Figure 5B). Unmodified circFOREIGN strongly stimulated MAVS polymerization in a concentration-dependent manner in the presence of K63-Ub$_n$ (Figure 5B). Importantly, when m^{6}A modification is incorporated onto circFOREIGN at 1% or 100%, the MAVS filamentation is substantially decreased or fully abro-

gated, respectively (Figures 5B and 5C). In the absence of K63-Ub$_n$, none of the circRNA substrates induced MAVS polymerization, indicating that polyubiquitin is necessary to stabilize activated RIG-I conformation for subsequent MAVS polymerization and signaling to occur (Figure S7D). Quantification of MAVS filaments by electron microscopy confirmed that unmodified circFOREIGN strongly induced MAVS filamentation, whereas m^{6}A modification of circFOREIGN suppressed the ability of MAVS to oligomerize (Figures 5B and 5C).

These *in vitro* results with purified components demonstrate that unmodified circFOREIGN can directly activate RIG-I in the presence of K63-Ub$_n$ and activate MAVS, in the absence of any other enzyme or RNA binding proteins. Although RIG-I binding fails to distinguish between unmodified and m^{6}A-modified circRNA (Figure S7C), only unmodified circFOREIGN initiates MAVS filamentation in the presence of K63-Ub$_n$ (Figures 5A–5C). These results suggest that m^{6}A discrimination is dependent on RIG-I conformational change, not in RIG-I binding, which is

subsequently read out in the MAVS monomer to filament transition.

CircFOREIGN Activates IRF3 Dimerization

Following MAVS filamentation, dimerization of the downstream transcription factor IRF3 completes the innate immune signaling to the genome. To test the ability of circFOREIGN to activate IRF3, we performed a cell-free assay by first forming the RIG-I, RNA, K63-Ub$_n$ complex, and then incubating with radiolabeled-IRF3 in the presence of cellular extract (S1) containing both cytosolic and mitochondrial fractions. CircFOREIGN strongly induced IRF3 dimerization in a concentration-dependent manner, whereas m^{6}A-modified circFOREIGN led to substantially less IRF3 dimerization (Figure 5D, lanes 5–7 versus lanes 8–10). The known agonist 5′-triphosphate 162 bp dsRNA stimulated RIG-I-mediated IRF3 dimerization better when it was present at a substoichiometric amount and increased dsRNA prevented effective oligomerization of RIG-I on RNA (Figure S7E). 5′-Hydroxyl linear RNA did not stimulate IRF3 dimerization, as expected of the negative control (Figure 5D, lanes 2–4).

CircFOREIGN Requires Proper Complex Formation Prior to Activation

To understand the requirements of RIG-I oligomerization and activation, we examined the order of addition of specific components for the *in vitro* assay. 5′-triphosphate RNA showed a more potent response when pre-incubated with RIG-I and K63-Ub$_n$ prior to the supplementation of S1 lysate and radiolabeled-IRF3. However, addition of 5′-triphosphate dsRNA after the introduction of S1 lysate and radiolabeled-IRF3 resulted in a reduced, albeit significant, stimulatory activity (Figure S7E, lanes 2 and 5 versus 8 and 9). We next examined the incubation of 5′-triphosphate dsRNA and RIG-I together, followed by addition of S1 lysate and radiolabeled-IRF3 with or without K63-Ub$_n$. K63-Ub$_n$ is not active at the S1 stage, as there is no difference between whether or not K63-Ub$_n$ is present (Figure S7E, lanes 12 and 13 versus 10 and 11). When we added circFOREIGN to S1 cellular lysate and then mixed with RIG-I and K63-Ub$_n$, no IRF3 dimerization activity resulted (Figure 5D, lanes 11–13). This result suggests that K63-Ub$_n$ needs to interact with and stabilize RIG-I in the presence of agonist circRNA first, possibly due to rapid degradation or destabilization of free K63-Ub$_n$ in cellular lysate. Therefore, the signaling complex needs to be pre-formed before the addition of S1 cellular lysate. An additional experiment rules out the role of endogenous RNAs in circFOREIGN-mediated activation of IRF3 (Figure S7F). Together, our biochemical reconstitution demonstrated that circFOREIGN, RIG-I, and K63-Ub$_n$ form a three-component signaling-competent complex for immune signaling.

Distinct Localization of Unmodified versus m^{6}A-Marked circRNAs in Cells

To validate the *in vitro* assay of RIG-I directly sensing circFOREIGN, we performed immunofluorescence microscopy. HeLa cells were transfected with fluorescein isothiocyanate (FITC)-labeled circFOREIGN, fixed with formaldehyde, and RIG-I and K63-Ub$_n$ were labeled (Figure 6A). The vast majority of unmodified circFOREIGN-FITC co-localized with both RIG-I

and K63-Ub$_n$ (Figure 6B, 85.5%). Interaction with unmodified circFOREIGN activates RIG-I when K63-Ub$_n$ is present in the complex, which allows subsequent stimulation of MAVS filamentation.
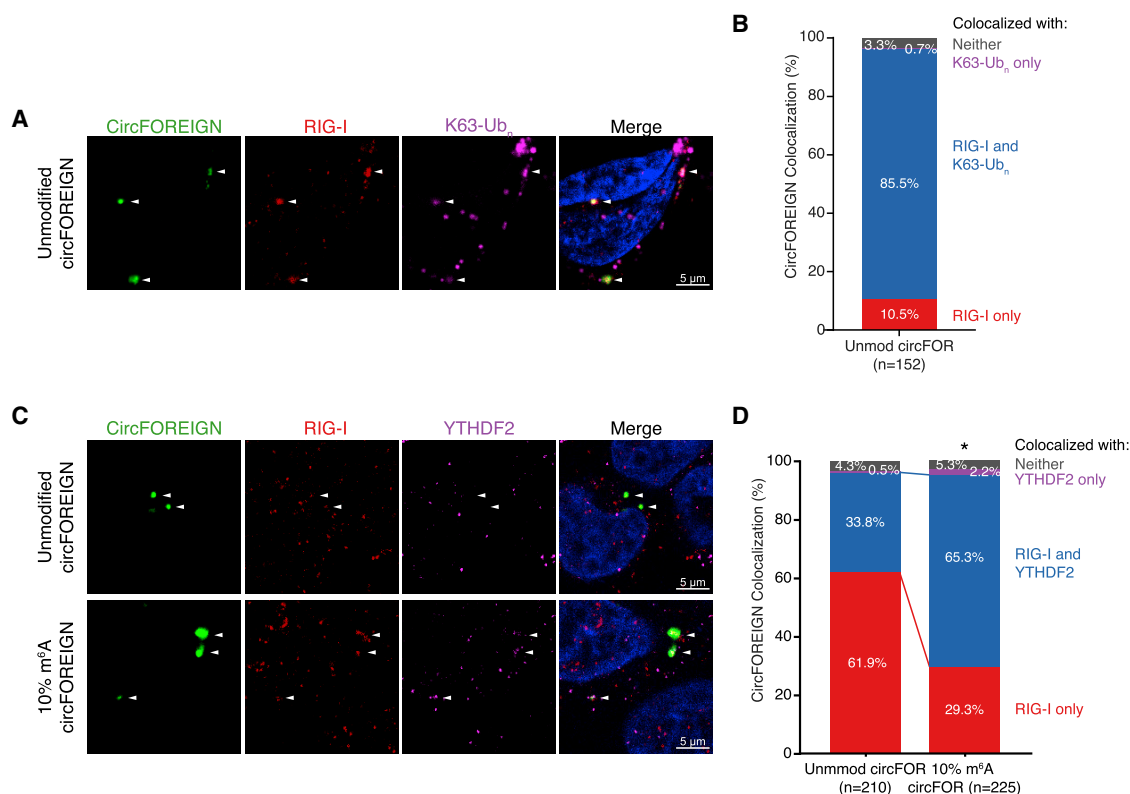
Because RIG-I activation discriminates between unmodified and m^{6}A-modified circRNA, we reasoned that YTHDF2 participates in the complex that either inhibits RIG-I activation or decreases RIG-I binding. We had previously used 1% m^{6}A modification on circRNA, but we anticipate that the m^{6}A level at RRACH consensus motif is much lower than 1% because the m^{6}A is randomly incorporated. YTHDF2 binds m^{6}A at RRACH motifs (Dominissini et al., 2012; Meyer et al., 2012). Thus, we incorporated 10% m^{6}A into circFOREIGN for better modeling of m^{6}A placement at consensus sequences. We performed immunofluorescence microscopy with unmodified or 10% m^{6}A-modified circFOREIGN, RIG-I, and YTHDF2 (Figure 6C). The percentage of circRNA co-localization with RIG-I and YTHDF2 is more than doubled when m^{6}A-modification is present on circFOREIGN (33.8% to 65.3%), whereas the percentage of circFOREIGN interacting with RIG-I alone decreased (Figure 6D, 61.9% to 29.3%). The results demonstrate that m^{6}A modification recruits YTHDF2 to the same complex with RIG-I. These immunofluorescence studies provide orthogonal and spatial information for the distinct fates of unmodified versus m^{6}A-modified circRNAs in cells.

Taken together, the data suggest that RIG-I recognizes foreign circRNA through a mechanism that is dependent on K63-Ub$_n$ (Figure 7). Forming the complex of RIG-I, unmodified RNA, and K63-Ub$_n$ triggers MAVS filamentation and IRF3 dimerization to stimulate interferon production downstream. m^{6}A-modified circFOREIGN also binds RIG-I but suppresses RIG-I activation, and thus self circRNAs that carry the m^{6}A modification can be safely ignored. In cells, YTHDF2 acts with m^{6}A to inhibit immune signaling.

DISCUSSION

The definition of self versus foreign is the fundamental challenge of any system of immunity. Mammalian cells possess elaborate mechanisms to monitor the ends of RNA transcripts. All transcripts generated by RNA polymerase II bear a 5′ m^{7}G cap, and RIG-I sense 5′-triphosphate for immune monitoring. In principle, circRNAs can bypass the end monitoring system because circRNAs have no ends. Although the functions of endogenous circRNAs are mostly not known, their large number and the presence of viral circRNA genomes necessitate a system of circRNA immunity. The recent discoveries of human circRNA modulation of viral resistance through regulation of NF90/NF110 (Li et al., 2017) and autoimmunity through PKR regulation (Liu et al., 2019) highlight this concept. We provide *in vivo* evidence that circRNA acts as potent adjuvants to induce specific T and B cell responses. We show that circRNA can induce both innate and adaptive immune responses and has the ability to inhibit the establishment and growth of tumors. The ability of circRNA to enter cells *in vivo* allows for potential development of immunotherapies that harness the stability, immunogenicity, and ability to encode proteins in circRNA sequences.

Although our results appear to contradict those of Wesselhoeft et al. (2019) at first glance, they may in fact converge on

Figure 6. Immunofluorescence Reveals CircFOREIGN Co-localization with RIG-I and K63-Ub$_n$ and YTHDF2 Recruitment to m^{6}A-Modified CircFOREIGN

(A) CircFOREIGN co-localizes with RIG-I and K63-Ub$_n$. Representative field of view is shown.

(B) Quantification of circFOREIGN colocalization with RIG-I and K63-Ub$_n$ (n = 152). Foci were collected across 10 fields of view and biological replicates and are representative of replicate experiments.

(C) 10% m^{6}A circFOREIGN has increased co-localization with YTHDF2. Representative field of view is shown. Foci were collected across more than 10 fields of view and representative of replicate experiments.

(D) Quantification of circFOREIGN and 10% m^{6}A circFOREIGN colocalization with YTHDF2 and RIG-I. *$p < 0.05$, Pearson's χ^2 test.

several common lessons. We found that exogenous circRNAs can activate RIG-I in comparison to phosphatase-treated linear RNA (Chen et al., 2017; this work). Wesselhoeft et al. (2019) reported that in the absence of phosphatase treatment, 5′ triphosphate-containing linear RNAs present in circRNA preparations are more immunogenic than circRNAs. Both results are consistent with our findings using purified RIG-I pathway components and dose titration of RNA ligands, quantifying MAVS polymerization or IRF3 dimerization as readouts. That is, circRNA is RIG-I-stimulatory, but it does not appear to be as strong as dsRNA with 5′-triphosphate. Thus, care should be taken for applications of circRNA as vehicles for gene delivery, but the immunogenicity of circRNA may also be exploited for therapeutic applications such as against cancer.

Our results suggest that human circRNAs are marked at birth, based on the introns that program their back splicing, by the covalent m^{6}A modification. We find that RIG-I discriminates between unmodified and m^{6}A-modified circRNAs and is only activated by the former. RIG-I is necessary and sufficient for innate immunity to foreign circRNA (Chen et al., 2017) while toll-like receptors are not responsive to circRNAs (Wesselhoeft et al.,

2019). In contrast, foreign circRNA lacking RNA modification is recognized by RIG-I and K63-Ub$_n$, and m^{6}A modification suffices to mark an otherwise foreign circRNA as "self" to prevent immune activation. Mutation of all adenosines, or just the adenosines in RRACH (the canonical m^{6}A motif), in a model circRNA substantially increased circRNA induction of anti-viral genes. These results provide the first evidence that specific circRNA exonic sequences impact immunity and specifically suggest endogenous m^{6}A modification dampens innate immunity. We speculate that an RRACH-less or A-less circSELF would also activate innate immunity, although this remains to be shown. m^{6}A modification of 5′-triphosphate linear RNA ligands also abrogates RIG-I binding and activation (Durbin et al., 2016; Peisley et al., 2013). Hence, RIG-I appears to be a general reader of circRNAs and its activation is suppressed by RNA modification, a predominant feature of eukaryotic RNAs. Both unmodified and m^{6}A circRNA can bind RIG-I, but only unmodified circRNA activates RIG-I to initiate MAVS filamentation. These results suggest RIG-I conformational changes are necessary to induce MAVS filamentation. This observation is analogous to the selectivity of RIG-I for 5′ triphosphate (present on viral RNAs) over m^{7}G cap

Figure 7. Model of CircRNA Induction of Innate Immune Response through RIG-I

Unmodified circRNA interacts with RIG-I in the presence of K63-Ub$_n$ to induce MAVS filamentation, which triggers IRF3 dimerization and interferon production. m^{6}A-modified circRNAs interacts with YTHDF2 and does not initiate RIG-I signaling.

(present on all mRNAs) due to conformational change rather than ligand binding (Devarkar et al., 2016). Co-crystal structure and biochemical analyses show that 5′ triphosphate and m^{7}G both bind RIG-I with the same affinity, but the latter triggers a distinct conformational change and causes RIG-I to filter against endogenous mRNAs and lowers ATPase activity (Devarkar et al., 2016). In living cells, YTHDF2 may inhibit the RIG-I conformational transitions necessary for downstream signaling of immune genes (Figure 6).

We systematically addressed the necessity, sufficiency, and domain requirements of YTHDF2-mediated suppression of circRNA immunity. The requirement of full-length YTHDF2 is consistent with recent model that YTH-proteins recruit m^{6}A-modified RNAs into phase-separated condensates via their N-terminal disordered domains (i.e., both domains are needed for higher-order RNA-protein interactions; Ries et al., 2019). Our results extend prior knowledge about YTHDF function. Although tethering just the effector domain is sufficient to induce RNA decay or translation (Wang et al., 2014, 2015), the full-length protein is needed for self-foreign discrimination of circRNAs. These results suggest a double-layered system for m^{6}A to both sequester and block endogenous circRNAs from activating the RIG-I antiviral pathway. These results have substantially increased our mechanistic understanding of the role of YTHDF2 in circRNA immunity. In addition to YTHDF2, there may also be other sensors and receptors involved in identifying endogenous circRNAs as self. Moreover, m^{6}A may also not be the only RNA

modification that impacts circRNA immunity, because other RNA modifications also modulate circRNA immunity (Figure S7G). Because over a hundred different RNA modifications have been discovered and characterized, endogenous circRNAs may contain more than one modification that regulates the cell's ability to identify self/non-self RNA. The logic of using nucleic acid chemical modification to distinguish self versus foreign genes, independent of sequence content, is strikingly similar for DNA modification-restriction systems recognized since the 1970s and circRNA immunity that we uncovered here.

STAR★METHODS

Detailed methods are provided in the online version of this paper and include the following:

- KEY RESOURCES TABLE
- LEAD CONTACT AND MATERIALS AVAILABILITY
- EXPERIMENTAL MODEL AND SUBJECT DETAILS
  - Cell lines and maintenance
  - Cell culture and transient transfection
  - Immunization of mice (for CD8$^+$ T cell FACS analysis, antibody ELISA, and Dendritic cell analysis)
- METHOD DETAILS
  - Plasmids
  - RNA synthesis and purification
  - m^{6}A-irCLIP
  - m^{6}A-RIP-seq
  - Reverse transcription and real time PCR analysis (qRT-PCR)
  - Western blot analysis
  - YTHDF2 rescue and YTHDF1/2 Tethering to circFOREIGN-BoxB
  - RNA immunoprecipitation-qPCR
  - METTL3 siRNA FACS analysis
  - CD8$^+$ T cell FACS analysis
  - Antibody ELISA
  - Dendritic cell analysis
  - RIG-I ATPase assay
  - RIG-I native gel shift assay
  - RIG-I polymerization assay
  - Protein Preparation
  - MAVS polymerization assay
  - Immunofluorescence and Quantification
  - IRF3 dimerization assay
  - Statistical Analyses
- DATA AND CODE AVAILABILITY

SUPPLEMENTAL INFORMATION

Supplemental Information can be found online at https://doi.org/10.1016/j.molcel.2019.07.016.

AUTHOR CONTRIBUTIONS

Y.G.C. and H.Y.C. conceived of the project. Y.G.C. and R.C. led the project, performed experiments, analyzed data, and wrote the manuscript with input of all authors. S.A., R.V., S.P.K., L.A., C.C., J.P.B., and J.K. performed experiments, analyzed data, and edited the manuscript. S.H. and B.P. provided key suggestions. H.Y.C. supervised the project, analyzed data, and wrote the manuscript with Y.G.C and input of all authors.

DECLARATION OF INTERESTS

Stanford University and Emory University have filed patent applications based on this work, and H.Y.C., Y.G.C., R.C., L.A., B.P., and S.P.K. are named as co-inventors. H.Y.C. is a co-founder and advisor of Accent Therapeutics and Boundless Bio. H.Y.C. is an advisor of 10X Genomics, Arsenal Biosciences, and Spring Discovery.

REFERENCES

Ahmad, S., Mu, X., Yang, F., Greenwald, E., Park, J.W., Jacob, E., Zhang, C.Z., and Hur, S. (2018). Breaching Self-Tolerance to Alu Duplex RNA Underlies MDA5-Mediated Inflammation. Cell 172, 797–810.

Baron-Benhamou, J., Gehring, N.H., Kulozik, A.E., and Hentze, M.W. (2004). Using the λN Peptide to Tether Proteins to RNAs. In mRNA Processing and Metabolism: Methods and Protocols, D.R. Schoenberg, ed. (Humana Press), pp. 135–153.

Batista, P.J., Molinie, B., Wang, J., Qu, K., Zhang, J., Li, L., Bouley, D.M., Lujan, E., Haddad, B., Daneshvar, K., et al. (2014). m(6)A RNA modification controls cell fate transition in mammalian embryonic stem cells. Cell Stem Cell 15, 707–719.

Budhu, S., Loike, J.D., Pandolfi, A., Han, S., Catalano, G., Constantinescu, A., Clynes, R., and Silverstein, S.C. (2010). CD8+ T cell concentration determines their efficiency in killing cognate antigen-expressing syngeneic mammalian cells in vitro and in mouse tissues. J. Exp. Med. 207, 223–235.

Chen, Y.G., Kim, M.V., Chen, X., Batista, P.J., Aoyama, S., Wilusz, J.E., Iwasaki, A., and Chang, H.Y. (2017). Sensing Self and Foreign Circular RNAs by Intron Identity. Mol. Cell 67, 228–238.

Devarkar, S.C., Wang, C., Miller, M.T., Ramanathan, A., Jiang, F., Khan, A.G., Patel, S.S., and Marcotrigiano, J. (2016). Structural basis for m7G recognition and 2′-O-methyl discrimination in capped RNAs by the innate immune receptor RIG-I. Proc. Natl. Acad. Sci. USA 113, 596–601.

Dominissini, D., Moshitch-Moshkovitz, S., Schwartz, S., Salmon-Divon, M., Ungar, L., Osenberg, S., Cesarkas, K., Jacob-Hirsch, J., Amariglio, N., Kupiec, M., et al. (2012). Topology of the human and mouse m6A RNA methylomes revealed by m6A-seq. Nature 485, 201–206.

Dong, K.C., Helgason, E., Yu, C., Phu, L., Arnott, D.P., Bosanac, I., Compaan, D.M., Huang, O.W., Fedorova, A.V., Kirkpatrick, D.S., et al. (2011). Preparation of distinct ubiquitin chain reagents of high purity and yield. Structure 19, 1053–1063.

Durbin, A.F., Wang, C., Marcotrigiano, J., and Gehrke, L. (2016). RNAs Containing Modified Nucleotides Fail To Trigger RIG-I Conformational Changes for Innate Immune Signaling. MBio 7, e00833-16.

Edupuganti, R.R., Geiger, S., Lindeboom, R.G.H., Shi, H., Hsu, P.J., Lu, Z., Wang, S.Y., Baltissen, M.P.A., Jansen, P.W.T.C., Rossa, M., et al. (2017). N6-methyladenosine (m6A) recruits and repels proteins to regulate mRNA homeostasis. Nat. Struct. Mol. Biol. 24, 870–878.

Flynn, R.A., Martin, L., Spitale, R.C., Do, B.T., Sagan, S.M., Zarnegar, B., Qu, K., Khavari, P.A., Quake, S.R., Sarnow, P., and Chang, H.Y. (2015). Dissecting noncoding and pathogen RNA-protein interactomes. RNA 21, 135–143.

Hansen, T.B., Jensen, T.I., Clausen, B.H., Bramsen, J.B., Finsen, B., Damgaard, C.K., and Kjems, J. (2013). Natural RNA circles function as efficient microRNA sponges. Nature 495, 384–388.

Hornung, V., Ellegast, J., Kim, S., Brzózka, K., Jung, A., Kato, H., Poeck, H., Akira, S., Conzelmann, K.K., Schlee, M., et al. (2006). 5′-Triphosphate RNA is the ligand for RIG-I. Science 314, 994–997.

Jiang, X., Kinch, L.N., Brautigam, C.A., Chen, X., Du, F., Grishin, N.V., and Chen, Z.J. (2012). Ubiquitin-induced oligomerization of the RNA sensors RIG-I and MDA5 activates antiviral innate immune response. Immunity 36, 959–973.

Ke, S., Alemu, E.A., Mertens, C., Gantman, E.C., Fak, J.J., Mele, A., Haripal, B., Zucker-Scharff, I., Moore, M.J., Park, C.Y., et al. (2015). A majority of m6A residues are in the last exons, allowing the potential for 3′ UTR regulation. Genes Dev. 29, 2037–2053.

Kos, A., Dijkema, R., Arnberg, A.C., van der Meide, P.H., and Schellekens, H. (1986). The hepatitis delta (delta) virus possesses a circular RNA. Nature 323, 558–560.

Legnini, I., Di Timoteo, G., Rossi, F., Morlando, M., Briganti, F., Sthandier, O., Fatica, A., Santini, T., Andronache, A., Wade, M., et al. (2017). Circ-ZNF609 Is a Circular RNA that Can Be Translated and Functions in Myogenesis. Mol. Cell 66, 22–37.

Li, X., Liu, C.X., Xue, W., Zhang, Y., Jiang, S., Yin, Q.F., Wei, J., Yao, R.W., Yang, L., and Chen, L.L. (2017). Coordinated circRNA Biogenesis and Function with NF90/NF110 in Viral Infection. Mol. Cell 67, 214–227.

Liu, C.X., Li, X., Nan, F., Jiang, S., Gao, X., Guo, S.K., Xue, W., Cui, Y., Dong, K., Ding, H., et al. (2019). Structure and Degradation of Circular RNAs Regulate PKR Activation in Innate Immunity. Cell 177, 865–880.

Memczak, S., Jens, M., Elefsinioti, A., Torti, F., Krueger, J., Rybak, A., Maier, L., Mackowiak, S.D., Gregersen, L.H., Munschauer, M., et al. (2013). Circular RNAs are a large class of animal RNAs with regulatory potency. Nature 495, 333–338.

Meyer, K.D., Patil, D.P., Zhou, J., Zinoviev, A., Skabkin, M.A., Elemento, O., Pestova, Tatyana, V., Qian, S.B., and Jaffrey, S.R. (2015). 5' UTR m6A Promotes Cap-Independent Translation. Cell 163, 999–1010.

Meyer, K.D., Saletore, Y., Zumbo, P., Elemento, O., Mason, C.E., and Jaffrey, S.R. (2012). Comprehensive analysis of mRNA methylation reveals enrichment in 3′ UTRs and near stop codons. Cell 149, 1635–1646.

Ohi, M., Li, Y., Cheng, Y., and Walz, T. (2004). Negative staining and image classification — powerful tools in modern electron microscopy. Biol. Proced. Online 6, 23–34.

Peisley, A., Wu, B., Yao, H., Walz, T., and Hur, S. (2013). RIG-I forms signaling-competent filaments in an ATP-dependent, ubiquitin-independent manner. Mol. Cell 51, 573–583.

Peisley, A., Wu, B., Xu, H., Chen, Z.J., and Hur, S. (2014). Structural basis for ubiquitin-mediated antiviral signal activation by RIG-I. Nature 509, 110–114.

Reikine, S., Nguyen, J.B., and Modis, Y. (2014). Pattern Recognition and Signaling Mechanisms of RIG-I and MDA5. Front. Immunol. 5, 342.

Ries, R.J., Zaccara, S., Klein, P., Olarerin-George, A., Namkoong, S., Pickering, B.F., Patil, D.P., Kwak, H., Lee, J.H., and Jaffrey, S.R. (2019). m6A enhances the phase separation potential of mRNA. Nature 571, 424–428.

Roundtree, I.A., Evans, M.E., Pan, T., and He, C. (2017). Dynamic RNA Modifications in Gene Expression Regulation. Cell 169, 1187–1200.

Rybak-Wolf, A., Stottmeister, C., Glažar, P., Jens, M., Pino, N., Giusti, S., Hanan, M., Behm, M., Bartok, O., Ashwal-Fluss, R., et al. (2015). Circular RNAs in the Mammalian Brain Are Highly Abundant, Conserved, and Dynamically Expressed. Mol. Cell 58, 870–885.

Salzman, J., Gawad, C., Wang, P.L., Lacayo, N., and Brown, P.O. (2012). Circular RNAs are the predominant transcript isoform from hundreds of human genes in diverse cell types. PLoS ONE 7, e30733.

Sanger, H.L., Klotz, G., Riesner, D., Gross, H.J., and Kleinschmidt, A.K. (1976). Viroids are single-stranded covalently closed circular RNA molecules existing as highly base-paired rod-like structures. Proc. Natl. Acad. Sci. USA 73, 3852–3856.

Schlee, M., and Hartmann, G. (2010). The chase for the RIG-I ligand–recent advances. Mol. Ther. 18, 1254–1262.

Schlee, M., Roth, A., Hornung, V., Hagmann, C.A., Wimmenauer, V., Barchet, W., Coch, C., Janke, M., Mihailovic, A., Wardle, G., et al. (2009). Recognition of 5′ triphosphate by RIG-I helicase requires short blunt double-stranded RNA as contained in panhandle of negative-strand virus. Immunity 31, 25–34.

Smith, T., Heger, A., and Sudbery, I. (2017). UMI-tools: modeling sequencing errors in Unique Molecular Identifiers to improve quantification accuracy. Genome Res. 27, 491–499.

Toptan, T., Abere, B., Nalesnik, M.A., Swerdlow, S.H., Ranganathan, S., Lee, N., Shair, K.H., Moore, P.S., and Chang, Y. (2018). Circular DNA tumor viruses make circular RNAs. Proc. Natl. Acad. Sci. USA 115, E8737–E8745.

Wang, X., Lu, Z., Gomez, A., Hon, G.C., Yue, Y., Han, D., Fu, Y., Parisien, M., Dai, Q., Jia, G., et al. (2014). N6-methyladenosine-dependent regulation of messenger RNA stability. Nature 505, 117–120.

Wang, X., Zhao, B.S., Roundtree, I.A., Lu, Z., Han, D., Ma, H., Weng, X., Chen, K., Shi, H., and He, C. (2015). N(6)-methyladenosine Modulates Messenger RNA Translation Efficiency. Cell 161, 1388–1399.

Wesselhoeft, R.A., Kowalski, P.S., Parker-Hale, F.C., Huang, Y., Bisaria, N., and Anderson, D.G. (2019). RNA Circularization Diminishes Immunogenicity and Can Extend Translation Duration In Vivo. Mol. Cell 74, 508–520.

Wu, B., and Hur, S. (2015). How RIG-I like receptors activate MAVS. Curr. Opin. Virol. 12, 91–98.

Wu, B., Peisley, A., Richards, C., Yao, H., Zeng, X., Lin, C., Chu, F., Walz, T., and Hur, S. (2013). Structural basis for dsRNA recognition, filament formation, and antiviral signal activation by MDA5. Cell 152, 276–289.

Wu, B., Huoh, Y.-S., and Hur, S. (2016). Measuring Monomer-to-Filament Transition of MAVS as an In Vitro Activity Assay for RIG-I-Like Receptors. In Toll-Like Receptors: Practice and Methods, C.E. McCoy, ed. (Springer New York), pp. 131–142.

Xiao, W., Adhikari, S., Dahal, U., Chen, Y.S., Hao, Y.J., Sun, B.F., Sun, H.Y., Li, A., Ping, X.L., Lai, W.Y., et al. (2016). Nuclear m(6)A Reader YTHDC1 Regulates mRNA Splicing. Mol. Cell 61, 507–519.

Yang, Y., Fan, X., Mao, M., Song, X., Wu, P., Zhang, Y., Jin, Y., Yang, Y., Chen, L., Wang, Y., et al. (2017). Extensive translation of circular RNAs driven by N6-methyladenosine. Cell Res. 27, 626–641.

Zarnegar, B.J., Flynn, R.A., Shen, Y., Do, B.T., Chang, H.Y., and Khavari, P.A. (2016). irCLIP platform for efficient characterization of protein-RNA interactions. Nat. Methods 13, 489–492.

Zeng, W., Sun, L., Jiang, X., Chen, X., Hou, F., Adhikari, A., Xu, M., and Chen, Z.J. (2010). Reconstitution of the RIG-I pathway reveals a signaling role of unanchored polyubiquitin chains in innate immunity. Cell 141, 315–330.

Zhou, C., Molinie, B., Daneshvar, K., Pondick, J.V., Wang, J., Van Wittenberghe, N., Xing, Y., Giallourakis, C.C., and Mullen, A.C. (2017). Genome-Wide Maps of m6A circRNAs Identify Widespread and Cell-Type-Specific Methylation Patterns that Are Distinct from mRNAs. Cell Rep. 20, 2262–2276.

STAR★METHODS

KEY RESOURCES TABLE

REAGENT or RESOURCE	SOURCE	IDENTIFIER
Antibodies		
β-Actin (8H10D10) Mouse mAb (1:9000 for WB)	Cell Signaling Technology	Cat# 3700S; RRID: AB_2242334
Anti-beta Actin antibody (1:1000 for WB)	Abcam	Cat# ab8227; RRID: AB_230518:
Monoclonal ANTI-FLAG® M2 antibody produced in mouse (1:1000 for WB)	Sigma-Aldrich	Cat# F1804; RRID: AB_262044
Anti-YTHDF1 antibody (1:1000 for WB)	Abcam	Cat# ab157542; RRID: N/A
YTHDF2 Polyclonal Antibody (1:250 for WB)	Thermo Fisher Scientific	Cat# PA5-63756; RRID: AB_2649742
Recombinant Anti-METTL3 antibody [EPR18810] (1:1500 for WB)	Abcam	Cat# ab195352; RRID: AB_2721254
Rig-I (D14G6) Rabbit mAb (1:200 for IF)	Cell Signaling Technology	Cat# 3743S; RRID: AB_2269233
Ub-K63 Monoclonal Antibody (HWA4C4) (1:200 for IF)	Thermo Fisher Scientific	Cat# 14-6077-82; RRID: AB_1257213
Mouse Anti-YTHDF2 polyclonal antibody (1:200 for IF)	USBiological Life Sciences	Cat# 135486; RRID: N/A
IRDye® 800CW Goat anti-Mouse IgG Secondary Antibody (1:15,000 for WB)	Li-COR Biosciences	Cat# 926-32210; RRID: AB_621842
IRDye® 800CW Goat anti-Rabbit IgG Secondary Antibody (1:15,000 for WB)	Li-COR Biosciences	Cat# 926-32211; RRID: AB_621843
IRDye® 680RD Goat anti-Mouse IgG Secondary Antibody (1:15,000 for WB)	Li-COR Biosciences	Cat# 926-68070; RRID: AB_10956588
IRDye® 680RD Goat anti-Rabbit IgG Secondary Antibody (1:15,000 for WB)	Li-COR Biosciences	Cat# 926-68071; RRID: AB_10956166
Goat anti-Rabbit IgG (H+L) Highly Cross-Adsorbed Secondary Antibody, Alexa Fluor Plus 594 (1:2000 for IF)	Thermo Fisher Scientific	Cat# A32740; RRID: AB_2762824
Goat anti-Mouse IgG (H+L) Highly Cross-Adsorbed Secondary Antibody, Alexa Fluor Plus 647 (1:2000 for IF)	Thermo Fisher Scientific	Cat# A32728; RRID: AB_2633277
m6A Polyclonal rabbit purified antibody	Synaptic Systems	Cat# 202 003; RRID: AB_2279214
Anti-FLAG® M2 Magnetic Beads	Sigma-Aldrich	Cat# M8823; RRID: AB_2637089
Brilliant Violet 711 anti-mouse CD8a Antibody (clone 53-6.7)	Biolegend	Cat# 100747; RRID: AB_11219594
Brilliant Violet 785 anti-mouse CD3 Antibody (clone 17A2)	Biolegend	Cat# 100231; RRID: AB_11218805
Brilliant Violet 650 anti-mouse CD4 Antibody (clone RM4-5)	Biolegend	Cat# 100555; RRID: AB_2562529
Purified Rat Anti-Mouse IFN-γ (clone XMG1.2)	BD Biosciences	Cat# 554409; RRID: AB_398550
Brilliant Violet 421 anti-mouse CD11c Antibody (clone N418)	Biolegend	Cat# 117329; RRID: AB_10897814
Brilliant Violet 650 anti-mouse/human CD11b Antibody (clone M1/70)	Biolegend	Cat# 101239; RRID: AB_11125575
Alexa Fluor® 700 anti-mouse I-A/I-E Antibody (clone M5/114.15.2)	Biolegend	Cat# 107621; RRID: AB_493726
FITC anti-mouse CD86 Antibody (clone PO3)	Biolegend	Cat# 105109; RRID: AB_313162
Brilliant Violet 605 anti-mouse CD45 Antibody (clone 30-F11)	Biolegend	Cat# 103155; RRID: AB_2650656
Goat Anti-Mouse IgG(H+L)-HRP	Southern Biotech	Cat# 1036-05; RRID: AB_2794348
Goat Anti-Mouse IgG$_1$-HRP	Southern Biotech	Cat# 1071-05; RRID: AB_2794426
Goat Anti-Mouse IgG$_{2c}$-HRP	Southern Biotech	Cat# 1078-05; RRID: AB_2794462
Bacterial and Virus Strains		
NEB® Turbo Competent *E. coli* (High Efficiency)	New England Biolabs	Cat# C2984H
Chemicals, Peptides, and Recombinant Proteins		
In-Fusion® HD Cloning Kit	Takara Bio	Cat# 638909
Fluorescein-12-UTP	Sigma-Aldrich	Cat# 11427857910
N6-Methyladenosine-5′-Triphosphate	TriLink Biotechnologies	Cat# N-1013

Continued

REAGENT or RESOURCE	SOURCE	IDENTIFIER
Pseudouridine-5′-Triphosphate	TriLink Biotechnologies	Cat# N-1019
Inosine-5′-Triphosphate	TriLink Biotechnologies	Cat# N-1020
FastAP	Thermo Fischer Scientific	Cat# EF0652
RNaseR	Lucigen	Cat# RNR07250
RNA Loading Dye, (2X)	New England Biolabs	Cat# B0363S
GeneRuler 1 kb DNA Ladder, ready-to-use	Thermo Fischer Scientific	Cat# SM0313
RiboRuler Low Range RNA Ladder, ready-to-use	Thermo Fischer Scientific	Cat# SM1833
T4 DNA Ligase	New England Biolabs	Cat# M0202M
DNase I	Ambion	Cat# AM2222
T4 PNK	New England Biolabs	Cat# M0201S
RNA Fragmentation Reagents	Thermo Fischer Scientific	Cat# AM8740
Ribolock RNase Inhibitor	Thermo Fischer Scientific	Cat# EO0382
TRIzol	Thermo Fischer Scientific	Cat# 15596018
Phenol:Chloroform:Isoamyl Alcohol 25:24:1 Saturated with 10 mM Tris, pH 8.0, 1 mM EDTA	Sigma-Aldrich	Cat# P2069
cOmplete Protease Inhibitor Cocktail	Sigma-Aldrich	Cat# 11697498001
Dynabeads Protein A for Immunoprecipitation	Thermo Fischer Scientific	Cat# 10002D
PEG 8000, Molecular Biology Grade (Polyethylene Glycol 8000)	Promega	Cat# V3011
DAPI	Thermo Fischer Scientific	Cat# D1306
Annexin V Binding Buffer, 10X concentrate	BD Biosciences	Cat# 556454
Annexin V, Alexa Fluor 647 conjugate	Thermo Fischer Scientific	Cat# A23204
Falcon® 5mL Round Bottom Polystyrene Test Tube, with Cell Strainer Snap Cap	Corning	Cat# 352235
Falcon® 40 μm Cell Strainer, Blue, Sterile,	Corning	Cat# 352340
Polyinosine-polycytidylic acid -TLR3 agonist	InvivoGen	Cat# vac-pic
EndoFit Ovalbumin	InvivoGen	Cat# vac-pova
Two OVA peptide standards for ELISPOT	InvivoGen	Cat# vac-sin
in vivo-jetPEI	Polyplus transfection	Cat# 201-10G
Corning® Matrigel® Growth Factor Reduced (GFR) Basement Membrane Matrix	Corning	Cat# 356231
D-Luciferin Firefly, potassium salt	Biosynth International	Cat# L-8220
Histopaque®-1083	Sigma-Aldrich	Cat# 10831
BD GolgiPlug Protein Transport Inhibitor (Containing Brefeldin A)	BD Biosciences	Cat# 555029
Nunc MaxiSorp flat-bottom	Thermo Fischer Scientific	Cat# 44-2404-21
Bovine Serum Albumin	Sigma-Aldrich	Cat# A9418-5G
1-Step Ultra TMB-ELISA Substrate Solution	Thermo Fischer Scientific	Cat# 34028
Stop Solution for TMB Substrates	Thermo Fischer Scientific	Cat# N600
Antibody Diluent	Thermo Fischer Scientific	Cat# 3118
VECTASHIELD® Antifade Mounting Medium with DAPI	Vector Laboratories	Cat# H-1200
Square Cover Glasses No. 1 1/2, Corning®	VWR	Cat# 89239-698
Lipofectamine 3000	Thermo Fischer Scientific	Cat# L3000008
Opti-MEM I Reduced Serum Medium	Thermo Fischer Scientific	Cat# 31985088
DMEM, high glucose, pyruvate	Thermo Fischer Scientific	Cat# 11995-073
Trypsin-EDTA (0.25%), phenol red	Thermo Fischer Scientific	Cat# 25200056
Penicillin-Streptomycin	Thermo Fischer Scientific	Cat# 15140-163
HyClone Characterized Fetal Bovine Serum (FBS), U.S. Origin	Thermo Fisher Scientific	Cat# SH30071.03
NuPAGE 4-12% Bis-Tris Protein Gels, 1.0 mm, 15-well	Thermo Fisher Scientific	Cat# NP0323BOX
NuPAGE MOPS SDS Running Buffer (20X)	Thermo Fisher Scientific	Cat# NP0001

Continued

REAGENT or RESOURCE	SOURCE	IDENTIFIER
2x Laemmli Sample Buffer	Bio-Rad Laboratories	Cat# 161-0737
Phosphate Buffered Saline with Tween® 20 (PBST-20X)	Cell Signaling Technologies	Cat# 9809
milliTUBE 1ml AFA Fiber	Covaris	Cat# 520130
RIG-I purified protein	Peisley et al., 2013	N/A
K63-Ub$_n$ purified protein	Dong et al., 2011	N/A
MAVS CARD-S purified protein	Wu et al., 2016	N/A
BIOMOL® Green	Enzo Life Sciences	Cat# BML-AK111-0250
SNAP-Surface® Alexa Fluor® 647	New England Biolabs	Cat# S9136S
^{35}S-IRF3	Ahmad et al., 2018	N/A
SYBR Gold Nucleic Acid Gel Stain (10,000X Concentrate in DMSO)	Thermo Fisher Scientific	Cat# S11494
Critical Commercial Assays		
ZymoPURE II Plasmid Prep Kits	Zymo Research	Cat# D4200
MEGAscript T7 Transcription Kit	Thermo Fisher Scientific	Cat# AM1334
Direct-zol RNA Miniprep	Zymo Research	Cat# R2051
RNeasy Mini Kit	QIAGEN	Cat# 74106
RNA Clean & Concentrator-5	Zymo Research	Cat# R1013
Zymoclean Gel Recovery Kit	Zymo Research	Cat# R1011
RiboMinus Eukaryote System v2 kit	Thermo Fisher Scientific	Cat# A15026
Poly(A)Purist MAG Kit	Thermo Fisher Scientific	Cat# AM1922
Brilliant II QRT-PCR Master Mix Kit, 1-Step	Agilent	Cat# 60080
Neon Transfection System 100 μL Kit	Thermo Fisher Scientific	Cat# MPK10025
RNA ScreenTape	Agilent	Cat# 5067-5576
RNA ScreenTape Sample Buffer	Agilent	Cat# 5067-5577
LIVE/DEAD Fixable Green Dead Cell Stain Kit, for 488 nm excitation	Thermo Fisher Scientific	Cat# L23101
BD Cytofix/Cytoperm Fixation/Permeabilization Solution Kit	BD Biosciences	Cat# 554714
Deposited Data		
m6A-irCLIP sequencing data	This paper	GEO: GSE116007
ChIRP-MS data	Chen et al., 2017	N/A
Experimental Models: Cell Lines		
HeLa	ATCC	Cat# CCL-2; RRID: CVCL_0030
HEK293T	ATCC	Cat# CRL-3216; RRID: CVCL_0063
RIG-I KO HeLa	Chen et al., 2017	N/A
YTHDF2 KO HeLa	Dr. Chuan He	N/A
Experimental Models: Organisms/Strains		
C57BL/6J mice	Jackson Laboratories	Cat# 000664; RRID: IMSR_JAX:000664
Oligonucleotides		
qRT-PCR primers	This paper	Table S1
irCLIP sequencing primers	Zarnegar et al., 2016	N/A
SMARTpool ON-TARGETplus METTL3 siRNA	Dharmacon	Cat# L-005170-02-0005
ON-TARGETplus Non-targeting Control siRNA #1	Dharmacon	Cat# D-001810-01-05
Recombinant DNA		
Plasmid: autocatalytic-splicing linear GFP-IRES (circGFPd2IRES)	Chen et al., 2017	N/A
Plasmid: circGFPd2IRES_N'5BoxB	This paper	pRC0050
Plasmid: pPB-CAG-Flag-GGS-lambda	Dr. Chuan He	N/A
Plasmid: pPB-CAG-Flag-YTHDF1N	Dr. Chuan He	N/A

Continued

REAGENT or RESOURCE	SOURCE	IDENTIFIER
Plasmid: pPB-CAG-Flag-YTHDF1N-lambda	Dr. Chuan He	N/A
Plasmid: pPB-CAG-Flag-YTHDF2N	Dr. Chuan He	N/A
Plasmid: pPB-CAG-Flag-YTHDF2N-lambda	Dr. Chuan He	N/A
Plasmid: pCAGGS-Flag-YTHDF1N	This paper	pRC0070
Plasmid: pCAGGS-Flag-YTHDF1N-GS-lambda	This paper	pRC0071
Plasmid: pCAGGS-Flag-YTHDF2N	This paper	pRC0103
Plasmid: pCAGGS-Flag-YTHDF2N-GS-lambda	This paper	pRC0104
Plasmid: pCAGGS-3xFlag-YTHdomain	This paper	pRC0151
Plasmid: pCAGGS-3xFlag-mRuby3-YTHdomain	This paper	pRC0152
Plasmid: pCAGGS-3xFlag-YTHdomain-GS-lambdaN	This paper	pRC0164
Plasmid: pCAGGS-3xFlag-mRuby3-YTHdomain-GS-lambdaN	This paper	pRC0165
Software and Algorithms		
ZEN (blue edition)	Carl Zeiss Microscopy	https://www.zeiss.com/microscopy/us/products/microscope-software/zen.html
FlowJo_V10	FlowJo, LLC	https://flowjo.com/solutions/flowjo/downloads

LEAD CONTACT AND MATERIALS AVAILABILITY

Further information and requests for resources and reagents should be directed to and will be fulfilled by the Lead Contact, Howard Y. Chang (howchang@stanford.edu).

EXPERIMENTAL MODEL AND SUBJECT DETAILS

Cell lines and maintenance

Human HeLa (cervical adenocarcinoma, ATCC CCL-2), human HEK293T (embryonic kidney, ATCC CRL-3216) cells, mouse B16/OVA (provided by Dr. Edith Lord, University of Rochester), and mouse B16/OVA/luciferase cells were grown in Dulbecco's modified Eagle's medium (DMEM, Invitrogen, 11995-073) supplemented with 100 units/ml penicillin-streptomycin (GIBCO, 15140-163) and 10% (v/v) fetal bovine serum (Thermo Fisher Scientific, SH30071.03). Cell growth was maintained at 37°C in a 5% CO_2 atmosphere, passaging at a 1:10 dilution every 2-3 days. B16/OVA/luciferase cells were generated by integrating a luciferase expression cassette into B16/OVA cells.

Cell culture and transient transfection

Cells were plated 24 hours prior to transfection. Cells were at 70 to 80% confluence and 500 ng of RNA was transfected into one well of a 24-well plate using Lipofectamine 3000 (Thermo Fisher Scientific, L3000008). The nucleic acids with P3000 and Lipofectamine 3000 were diluted in Opti-MEM (Thermo Fischer Scientific, 31985088) per manufacturer's instructions, and incubated for 3 minutes at room temperature. The nucleic acids and Lipofectamine 3000 were the mixed together, incubated for 20 minutes at room temperature and then the nucleic acids-Lipofectamine 3000 complexes were applied dropwise to the monolayer cultures.

When ectopic protein expression prior to RNA transfection was necessary, cells were electroporated with NEON Transfection System (Thermo Fisher Scientific MPK5000S) per manufacturer's instructions. In most cases, cells were resuspended in buffer R at 2×10^7/mL and 5 μg of DNA plasmid was electroporated with a 100 μL NEON tip. Electroporation parameters were 1,000V, 35ms pulse, and 2 pulses for HeLa cells. 12 hours later, cells were passaged and plated such that 24 hours later they would be at 70 to 80% confluent. 24 hours later, cells were then transfected with RNA with Lipofectamine 3000 as described above. 24 hours after transfection, cells were washed once with PBS and 300 μL of TRIzol reagent was added per 24-well. RNA was harvested with Direct-zol kit (Zymo Research).

Immunization of mice (for CD8^{+} T cell FACS analysis, antibody ELISA, and Dendritic cell analysis)

Eight-to-twelve-week-old female C57BL/6 mice purchased from Jackson Laboratories were immunized subcutaneously at the base of the tail with 100 μg per mouse of OVA protein (Invivogen, vac-pova) adjuvanted with 25 μg of HMW vaccine grade Poly I:C (Invivogen, vac-pic), 25 μg of circular RNA alone or with *in vivo*-jetPEI (Polyplus Transfection, 201-10G), 25 μg of modified RNA alone or with *in vivo*-jet PEI. PEI/RNA complexes were formulated as per the manufacturer's instructions. Mice were bled via the lateral tail or

facial vein at regular intervals for analysis of CD8^{+} T cell and antibody responses after vaccination as indicated in the figures. A booster vaccination after 5 weeks of primary vaccination was given where indicated. For tumor establishment and proliferation studies, 0.5 million OVA-expressing B16 melanoma cells with an integrated luciferase expression cassette (B16/OVA/luciferase) were delivered with matrigel (Corning, 356231) in the right and left flanks of mice fourteen days after a single RNA vaccination. Tumors were measured twice a week and bioluminescence was measured once a week. Bioluminescence was measured by injecting 3 mg per 20 g mouse of D-luciferin (Biosynth International, L-8220) intraperitoneally and imaged at 20 s to 1 minute range of exposure using Ami HT imager (Spectral Instruments). All animal procedures were performed in accordance with guidelines established by Stanford university institutional animal care and use committee guidelines.

METHOD DETAILS

Plasmids

Plasmid encoding phage introns that express circRNA through autocatalytic splicing was previously described in Chen et al. (2017). In-Fusion HD assembly (Takara Bio, 638910) was used to construct the plasmid encoding phage introns expressing foreign circGFP with BoxB motif (GCCCTGAAGAAGGGC) separated with short 9-44 bp variable spacer sequences to prevent recombination. The full sequence of the 5 BoxB cassette is as follows:

ttccctaagtccaactactaaactggggattcctggGCCCTGAAGAAGGGCccctcgactaagtccaactactaaactggGCCCTGAAGAAGGGCccatata ggGCCCTGAAGAAGGGCcctatcgaggatattatctcgactaagtccaactactaaactggGCCCTGAAGAAGGGCccatataggGCCCTGAAGAAG GGCcctatcgaggatattatctcgag.

Plasmids expressing YTHDF1N and YTHDF2N with and without lambdaN (DAQTRRRERRAEKQAQWKAAN) were provided by Dr. Chuan He (University of Chicago). Plasmids expressing YTHDF2 protein domain truncations were constructed with In-Fusion HD assembly. All plasmids were propagated in NEB Turbo Competent *E. coli* cells (NEB, C2984H) grown in LB medium and purified using the ZymoPURE II Plasmid Prep Kits (Zymo Research, D4200). Plasmids are available upon request.

RNA synthesis and purification

RNA was synthesized by *in vitro* transcription using MEGAscript T7 transcription kit (Ambion, AM1334) following the manufacturer's instructions and incubation at 37°C overnight, or for at least 8 hours. m[6]A-labeled RNA was synthesized in the same way by *in vitro* transcription using MEGAscript T7 transcription kit (Ambion, AM1334) and adding m[6]ATP (Trilink, N-1013) in the specified ratio with the transcription kit's ATP. Transcribed circFOREIGN was purified by RNeasy Mini column (QIAGEN, 74106), then treated with RNase R (Epicenter, RNR07250) in the following manner: circFOREIGN secondary structure was denatured at 72°C for 5 minutes followed by 2 minutes on ice; RNaseR was added at a ratio of 1U: 1 ug of RNA and incubated at 37°C for 2-3 hours. CircRNALinear RNA was not treated with RNase R. CircFOREIGN was then purified by RNeasy column. CircFOREIGN or linear RNA were then phosphatase treated by FastAP in the following manner: FastAP was added at a ratio of 1U: 1ug of circFOREIGN, incubated at 37°C for 2 hours, then purified by RNeasy column. RNA quality was assessed by Tapestation analysis (Agilent, 5067-5576).

CircFOREIGN was gel purified by first denaturing at 72°C for 3 minutes followed by 2 minutes on ice. RNA loading dye (New England Biolabs, B0363S) was then added and the RNA-dye mix was then loaded on a 1% low melting point agarose gel. Gel extraction was done on a blue light transilluminator (Clare Chemical) followed by Zymoclean Gel Recovery Kit (Zymo Research, R1011) purification following the manufacturer's instructions except for melting, which was done rotating at room temperature for 10 minutes to better preserve RNA integrity.

HPLC fractionation was performed with a 4.6 × 300mm size exclusion column (Sepax Technologies, 215980P-4630) with particle size of 5um and pore size of 2000 Å. Nuclease-free TE buffer was used as the mobile phase at a flow rate of 0.3 mL/minute. RNA fractions were manually collected, lyophilized, and then cleaned with RNA Clean & Concentrator-5 (Zymo Research, R1013) prior to subsequent quality control and experimental use.

m[6]A-irCLIP

10 μg of total RNA was enriched for circRNA by removing mRNAs (polyA-) using the Poly(A)Purist MAG Kit (Thermo Fisher Scientific, AM1922) and removing ribosomal RNAs (ribo-) using the RiboMinus Eukaryote System v2 kit (Thermo Fisher Scientific, A15026). The resulting polyA-/ribo- RNA was then fragmented to 35-100 nt sizes using the RNA Fragmentation Buffer (Thermo Fisher Scientific, AM8740) at 75°C for 12 minutes. Fragmented RNA was denatured and then incubated with anti-m[6]A antibody (Synaptic Systems, 202003) for 2 hours at 4°C in IPP buffer (50 mM Tris-HCl, pH 7.4; 100 mM NaCl; 0.05% NP-40; 5 mM EDTA). The RNA and antibody were then crosslinked using UV light (254 nm) using 2 rounds of crosslinking at 0.15J (Stratalinker 2400). The crosslinked RNA and antibody were then incubated with Protein A Dynabeads (Thermo Fisher Scientific, 10002D) for 2 hours at 4°C. The beads were then washed with once with IPP buffer for 10 minutes at 4°C with rotation, once with low salt buffer (50 mM Tris, pH 7.4; 50 mM NaCl; 1 mM EDTA; 0.1% NP-40) for 10 minutes at 4°C with rotation, once with high salt buffer (50 mM Tris–HCl pH 7.4, 1M NaCl, 1% NP-40, 0.1% SDS) for 10 minutes at 4°C with rotation, transferred to a new 1.5 mL tube, and washed twice with PNK buffer (20 mM Tris-HCl, pH 7.4; 10 mM MgCl$_2$; 0.2% Tween 20). Libraries were then prepared using the irCLIP method (Zarnegar et al., 2016). Libraries were

checked for quality by Bioanalyzer and submitted for sequencing on NextSeq 500 with custom sequencing primer P6_seq, as described in the irCLIP method. Reads were mapped to the hg38 and subsequently to a custom assembly of the circGFP sequence and PCR duplicates were removed using UMI-tools (Smith et al., 2017). Reproducible RT stops were identified using the FAST-iCLIP pipeline (Flynn et al., 2015).

m⁶A-RIP-seq

10 μg of total RNA was enriched for circRNA by removing mRNAs (polyA-) using the Poly(A)Purist MAG Kit (Thermo Fisher Scientific) and removing ribosomal RNAs (ribo-) using the RiboMinus Eukaryote System v2 kit (Thermo Fisher Scientific). The remaining RNA was then treated with RNase R to remove residual linear RNAs. The polyA-/ribo- RNase R+ RNA was then fragmented for 12 minutes at 75°C with RNA Fragmentation Buffer (Thermo Fisher Scientific). 3 μg anti-m⁶A (Synaptic Systems) was bound to Protein A Dyna-beads (Thermo Fisher Scientific) for 2 hours at room temperature. Antibody bound beads were then washed with IPP buffer (50mM Tris-HCl, pH 7.4; 100mM NaCl; 0.05% NP-40; 5mM EDTA) and resuspend in IPP with 1 μL RiboLock (Thermo Fisher Scientific, EO0382). Fragmented RNA in IPP buffer was incubated with antibody and beads for 2 hours at 4°C with rotation. RNA-bound beads were then washed once with IPP buffer for 10 minutes at 4°C with rotation, once with low-salt buffer (50 mM Tris, pH 7.4; 50 mM NaCl; 1 mM EDTA; 0.1% NP-40) for 5 minutes at 4°C with rotation, once with high-salt buffer (50 mM Tris–HCl pH 7.4, 1M NaCl, 1% NP-40, 0.1% SDS) for 5 minutes at 4°C with rotation. Beads were then resuspended in 300 μL high-salt buffer and transfer to a new 1.5 mL tube. Beads were washed with PNK buffer (20 mM Tris-HCl, pH 7.4; 10 mM MgCl₂; 0.2% Tween 20) and then resuspended in 500 μL Trizol and incubated for 5 minutes at 25°C. 150 μL chloroform:isoamyl alcohol was added and mixed before incubating at 25°C for 2 minutes. After spinning at 13,000xg at 4°C for 10 minutes, the aqueous layer was transferred to a new 1.5 mL tube and cleaned up with RNA Clean & Concentrator-5 (Zymo Research, R1013), R1013. RNA was eluted in 10 μL nuclease-free water. To eluted RNA and 10% input RNA, 10 μL of end-repair mix was added (4 μL 5X PNK buffer; 1 μL RiboLock, 1 μL FastAP; 2 μL T4 PNK, 2 μL nuclease-free water). Reaction was incubated at 37°C for 1 h. 20 μL of linker ligation mix (2 μL 10X RNA ligation buffer; 2 μL 100 mM DTT; 2μL L3 linker (Zarnegar et al., 2016); 2 μL T4 RNA ligase buffer; 12 μL PEG8000 50% w/v). Reaction was incubated for 3 hours at 25°C and then cleaned up with an RNA Clean & Concentrator-5 column. Processed RNA was eluted in 10 μL of nuclease-free water. Libraries were prepared using the irCLIP method (Zarnegar et al., 2016) and sequenced on a NextSeq 500 using a custom sequencing primer (P6_seq) (Zarnegar et al., 2016). Reads were aligned to hg38 and circGFP sequence. Bam files were normalized to genome mapped reads.

Reverse transcription and real time PCR analysis (qRT-PCR)

Total RNA was isolated from cells using TRIzol (Invitrogen, 15596018) and Direct-zol RNA Miniprep (Zymo Research, R2052) with on-column DNase I digestion, following the manufacturer's instructions. qRT-PCR analysis was performed in triplicate using Brilliant II SYBR Green qRT-PCR Master Mix (Agilent, 600825) and a LightCycler 480 (Roche). qRT-PCR primers used are found in Table S1. mRNA levels were normalized to beta-actin. Relative expression of indicated mRNA genes for RNA transfection are normalized by level of transfected RNA and plotted as the fold change to the expression level of cells with mock transfection.

Western blot analysis

Cells were collected and lysed 24 hours after transfection to extract total proteins. Bioruptor sonication with RIPA buffer (150 mM NaCl, 1% Triton X-100, 0.5% sodium deoxycholate, 0.1% SDS, 50 mM Tris, pH 8.0) was used to lyse the cells. Proteins were fractionated by sodium dodecyl sulfate polyacrylamide gel electrophoresis (SDS-PAGE), transferred to nitrocellulose membranes, blocked in phosphate-buffer saline containing 4% (wt/vol) nonfat milk for 1 hour rocking at room temperature, and then incubated overnight at 4°C with the indicated primary antibody. YTHDF2⁻/⁻ KO cells were validated with 1:250 YTHDF2 polyclonal antibody (Thermo Fisher Scientific, PA5-63756). Ectopic protein expression was validated with 1:1000 Flag M2 monoclonal antibody (Sigma-Aldrich F1804). Secondary antibodies were incubated for 1 hour at 1:15,000, in pairs depending on the primary antibody identities: IRDye® 800CW Goat anti-Mouse IgG (Li-COR Biosciences, 926-32210), IRDye® 800CW Goat anti-Rabbit IgG (Li-COR Biosciences, 926-32211), IRDye® 680RD Goat anti-Mouse IgG (Li-COR Biosciences, 926-68070), IRDye® 680RD Goat anti-Rabbit IgG (Li-COR Biosciences, 926-68071). Western blot detection and quantification was done using an Odyssey infrared imaging system (Li-COR Biosciences).

YTHDF2 rescue and YTHDF1/2 Tethering to circFOREIGN-BoxB

As described above, plasmids expressing YTHDF1N or YTHDF2N with and without λN were electroporated into cells via NEON Transfection System. After 12 hours later, cells were passaged and plated such that 24 hours later they would be at 70 to 80% confluent. 24 hours after this, 500 ng of circBoxB (circRNA with 5 BoxB sites) was transfected with Lipofectamine 3000. RNA was harvested and qRT-PCR was performed with Brilliant II SYBR Green qRT-PCR Master Mix and a LightCycler 480 as described above. Extra duplicates were set aside for protein lysate collection and ectopic protein expression in these conditions was simultaneously confirmed via western blot.

RNA immunoprecipitation-qPCR

Plasmids expressing Flag-tagged YTHDF1N or YTHDF2N with and without a lambdaN peptide tag were electroporated into cells via NEON Transfection System, then later passaged into 6-well format in a timeline described above. Approximately 3 million cells were harvested with 0.25% Trypsin-EDTA (Thermo Fisher Scientific, 25200056), then washed with PBS. Cells were then lysed in cell lysis buffer (50 mM Tris pH 8.0, 100 mM NaCl, 5 mM EDTA, 0.5% NP-40 with proteinase inhibitor) by Covaris Ultrasonicator with the following settings: Fill Level 10, Duty Cycle 5%, Peak Incident Power 140 W, Cycles/Burst 200, time per tube 300 s. Cell lysate was pelleted for 15 minutes at 16,000 rcf. Supernatant was collected and incubated with 100 μL of Anti-FLAG M2 Magnetic Beads (Sigma-Aldrich, M8823-5ML) for 2 hours rotating at room temperature to pull down YTHDF1N or YTHDF2N. Beads were washed three times with cell lysis buffer and one time with PBS. Beads were resuspended in 500 μL of TRIzol and total RNA was extracted using an RNeasy Mini kit (QIAGEN, 74106). qRT-PCR was performed with Brilliant II SYBR Green qRT-PCR Master Mix and a LightCycler 480 as described above. RNA levels were normalized as percent of input within each biological replicate. Results are presented as the fold change of the enrichment of circRNA over actin.

METTL3 siRNA FACS analysis

Cells were seeded into 24-well format at 60,000 cells per well in DMEM with FBS without antibiotics. After 24 hours, cells were transfected with siRNA per manufacturer's recommendations. Dharmafect SMARTpool ON-TARGETplus METTL3 siRNA (Dharmacon, L-005170-02-0005) was used as the knockdown siRNA and ON-TARGETplus Non-targeting Control siRNAs (Dharmacon, D-001810-01-05) was used as the non-targeting siRNA. Media was refreshed at 12 and 36 hours following transfection. 48 hours after transfection, cells were collected via 0.25% Trypsin-EDTA, stained with Annexin V-647 (Thermo Fisher Scientific, A23204) in Annexin Binding Buffer (BD Biosciences, 556454) for 15 minutes. Cells were then spun down and re-suspended into DAPI in Annexin Binding Buffer for 5 minutes. Cells were then resuspended in Annexin Binding Buffer without stain and passed through Round-Bottom Tubes with Cell Strainer Cap (Corning, 352235). Flow analysis was done on a special order FACS Aria II (BD Biosciences, Stanford Shared FACS Facility). Cells subject to the same transfection as above were collected and protein lysate was collected. METTL3 knockdown was confirmed via western blot using 1:1500 anti-METTL3 antibody (Abcam, ab195352). RIG-I protein expression was assayed via western blot using 1:1000 RIG-I monoclonal antibody (Abcam, ab180675).

CD8^{+} T cell FACS analysis

Primary and memory CD8^{+} T cell responses were evaluated at day 7 after primary and secondary immunizations. Briefly, peripheral blood mononuclear cells (PBMCs) were enriched using a Histopaque-1083 sucrose density gradient separation (Sigma-Aldrich 10831) and cultured with OVA-specific MHC class I restricted peptide at 1 μg/mL (SIINFEKL) (Invivogen, vac-sin) for restimulation ex-vivo in the presence of BD Golgi Plug TM (BD Biosciences, 555029) for 5 hours. Stimulated cells were first stained for surface markers anti-mouse CD8α (Biolegend, 100747), anti-mouse-CD3 (Biolegend, 100231), anti-mouse CD4 (Biolegend, 100555) followed by fixation in BD cytofix/cytoperm and intracellular staining (BD Biosciences, 554714) with anti-mouse IFN-γ (BD Biosciences, 554409), in BD cytoperm buffer. Dead cell was excluded using live/dead aqua stain (Thermo Fisher Scientific, L23101). Labeled cells were acquired on a special order FACS Aria II (BD Biosciences, Stanford Shared FACS Facility) and data were analyzed using Flow JO software (TreeStar).

Antibody ELISA

Nunc MaxiSorp 96 -well plates (Thermo Fisher Scientific, 44-2404-21) were coated with 100 μl of 20 μg/mL of OVA protein (Invivogen) overnight at 4°C. Plates were washed 3 times with PBS/0.5% Tween-20 using a Bio-Rad auto plate washer and blocked with 200 μl of 4% BSA (Sigma Aldrich, A9418-5G) for 2 hours at room temperature. Serum samples from immunized mice at the indicated time points were serially diluted in 0.1% BSA in PBS/0.5% Tween-20 and incubated on blocked plates for 2 hours at room temperature. Wells were washed and incubated with 1:5000 anti-mouse IgG-HRP (Southern Biotech, 1036-05), 1:5000 anti-mouse IgG$_1$–HRP conjugate (Southern Biotech, 1071-05) and 1:2000 anti-mouse IgG$_{2c}$–HRP conjugate (Southern Biotech, 1078-05) in PBS/0.5% Tween-20 for 2 hours at room temperature. Plates were washed and developed using 100 μl per well of tetramethylbenzidine (TMB) substrate (Thermo Fisher Scientific, 34028), followed by stopping the reaction using stop solution (Thermo Fisher Scientific, N600). Plates were analyzed using a Bio-Rad plate reading spectrophotometer at 450 nm with correction at 595 nm. Antibody titers were represented as serum reciprocal dilution yielding a > 0.3 optical density (OD) value at 450 nm.

Dendritic cell analysis

Mice were immunized with PBS (control) or circRNA (25 ug/mice) subcutaneously at base of the tail. 24 hours after the immunization mice were euthanized, skin draining inguinal lymph nodes were excised. Skin draining inguinal lymph nodes were gently busted with a 3 mL syringe plunger thumb rest, and digested with 1 mg/mL collagenase type 4 for 20-25 minutes at 37°C. Reactions were stopped with 2 mM EDTA and single cell suspension were prepared by passing through 40 μm cell strainers (Corning, 352340). The following staining antibodies were used:

Antibody	Clone	fluorochrome
CD11c	N418	BV421
CD11b	M1/70	BV650
CD103	2E7	PE/BB710
MHCII	M5/114.15.2	Alexa 700
CD86	PO3	FITC
CD45	30-F11	BV605

RIG-I ATPase assay

0.1 μM RIG-I was pre-incubated with the specified circular RNA or 512 bp 5′-triphosphate dsRNA (0.4 ng/μl) in buffer B (20 mM HEPES pH 7.5, 150 mM NaCl, 1.5 mM $MgCl_2$). The reaction was initiated by adding 2 mM ATP at 37°C. Aliquots (10 μl) were withdrawn at 2, 4, or 8 minutes after ATP addition, and immediately quenched with 100 mM EDTA. The ATP hydrolysis activity was measured using BIOMOL® Green Reagent (Enzo Life Sciences, AK111-0250). The Green Reagent (90 μl) was added to the quenched reaction at a ratio of 9:1, and OD650 was measured using a Synergy2 plate reader (BioTek).

RIG-I native gel shift assay

RNA (1 ng/uL) was incubated with RIG-I (500nM) in buffer A (20 mM HEPES pH 7.5, 50 mM NaCl, 1.5 mM $MgCl_2$, 2 mM ATP, and 5 mM DTT) at room temperature for 15 minutes. Poly-ubiquitin was then added at the indicated concentration and incubated at room temperature for 5 minutes. The complex was analyzed on Bis-Tris native PAGE gel (Life Technologies) and was stained with SybrGold stain (Thermo Fisher Scientific, S11494). SybrGold fluorescence was recorded using the scanner FLA9000 (Fuji) and analyzed with Multigauge (GE Healthcare).

RIG-I polymerization assay

0.4 μM RIG-I was incubated with the specified circular RNAs (1 ng/μl) in buffer A (20 mM HEPES pH 7.5, 50 mM NaCl, 1.5 mM $MgCl_2$, 2 mM ATP, and 5 mM DTT) at room temperature for 15 minutes. Prepared samples were adsorbed to carbon-coated grids (Ted Pella) and stained with 0.75% uranyl formate. Images were collected using a Tecnai G2 Spirit BioTWIN transmission electron microscope at 30,000x or 49,000x magnification.

Protein Preparation

Human RIG-I was expressed as previously reported (Peisley et al., 2013). Briefly, the proteins were expressed in BL21(DE3) at 20°C for 16-20 hours following induction with 0.5 mM IPTG. Cells were homogenized using an Emulsiflex C3 (Avestin), and the protein was purified three-step protocol including Ni-NTA, heparin affinity chromatography and size exclusion chromatography (SEC) in 20 mM HEPES, pH 7.5, 150 mM NaCl and 2 mM DTT.

K63-Ub_n was synthesized as previously reported (Dong et al., 2011). Briefly, mouse E1, human Ubc13, Uev1a and ubiquitin were purified from BL21(DE3), and were mixed in a reaction containing 0.4 mM ubiquitin, 4 μM mE1, 20 μM Ubc13 and 20 μM Uev1a in a buffer, 10 mM ATP, 50 mM Tris pH 7.5, 10 mM $MgCl_2$, 0.6 mM DTT. After incubating the reaction overnight at 37°C, synthesized K63-Ub_n chains were diluted 5-fold into 50 mM ammonium acetate pH 4.5, 0.1 M NaCl and separated over a 45 mL 0.1-0.6 M NaCl gradient in 50 mM ammonium acetate pH 4.5 using a Hi-Trap SP FF column (GE Healthcare). High molecular weight fractions were applied to an S200 10/300 column equilibrated in 20 mM HEPES pH 7.5, 0.15 M NaCl.

MAVS CARD was expressed as a fusion construct with the SNAP tag (CARD-S) in BL21(DE3) at 20°C for 16-20 hours following induction with 0.4 mM IPTG. The SNAP tag allows fluorescent labeling of MAVS CARD. MAVS CARD-S fusion was purified using Ni-NTA affinity chromatography as described (Wu et al., 2016), with the exception of using 0.05% NP-40 instead of CHAPS. Purified CARD-S was denatured in 6 M guanidinium hydrochloride for 30 minutes at 37°C with constant shaking, followed by dialysis against refolding buffer (20 mM Tris, pH 7.5, 500 mM NaCl, 0.5 mM EDTA and 20 mM BME) at 4°C for 1 hour. Refolded CARD-S was passed through a 0.1μ filter and subsequently fluorescently labeled with Alexa647-benzylguanine (New England Biolabs, S9136S) on ice for 15 minutes according to the manufacturer's instructions. The labeled MAVS CARD-S was immediately used for polymerization assay.

MAVS polymerization assay

The MAVS filament formation assay was performed as previously reported (Wu et al., 2013). MAVS CARD fused to SNAP (CARD-S) was labeled with BG-Alexa 647 (New England Biolabs) on ice for 15 minutes. RIG-I (1 μM) was pre-incubated with various concentrations of RNA and 2 mM ATP in the presence or absence of 6 μM K63-Ub_n in (20 mM HEPES pH 7.5, 150 mM NaCl, 1.5 mM $MgCl_2$, 2 mM DTT) for 15 minutes at room temperature. Subsequently, labeled monomeric MAVS CARD-S (10 μM) was added to the mixture and incubated further for 1 hour at room temperature. MAVS filament formation was detected by native PAGE analysis or by negative-stain EM. Prior to running on Bis-Tris gel (Life Technologies Corp.), all the samples were subjected to one round of freeze-thaw cycle

by incubating on dry ice for 5 minutes followed by incubation at room temperature for 5 minutes. Fluorescent gel images were scanned using an FLA9000 scanner (Fuji). Samples from MAVS polymerization assay were adsorbed to carbon-coated grids (Ted Pella) and stained with 0.75% uranyl formate as described previously (Ohi et al., 2004). Images were collected using a Tecnai G^2 Spirit BioTWIN transmission electron microscope at 9,300x magnification.

Immunofluorescence and Quantification

FITC-labeled RNA was synthesized as described above, except for the substitution of 5% Fluorescein 12 UTP (Thermo Fisher Scientific, 11427857910) for 100% UTP in the *in vitro* transcription reaction mix. 10% m^{6}A FITC-labeled RNA was synthesized with the additional substitution of 10% m^{6}A for 100% ATP in the *in vitro* transcription reaction mix. RNaseR and FastAP treatment were carried out as described. RNA quality was assessed via Tapestation.

HeLa cells were seeded on 22x22mm #1.5 thickness coverslips in 6-well format. After 12 hours, transient transfection of FITC-labeled circRNA was performed with Lipofectamine 3000 (Thermo Fisher Scientific, L3000015). After 12 hours, cells were fixed with 1% formaldehyde in PBS (Thermo Fisher Scientific, 28908) for 10 minutes at RT. The formaldehyde fixed slide was rinsed in PBS and permeabilized in 0.5% Triton X-100 in PBS for 10 minutes at RT. After the permeabilization solution was rinsed, the slide was blocked with antibody diluent (Thermo Fisher Scientific, 003118) for 1 hour at room temperature. Anti-RIG-I rabbit polyclonal primary antibody (Cell Signaling Technology, 3743S) and anti-Ub-K63 mouse monoclonal antibody (eBioscience, 14-6077-82) were diluted at 1:200 in antibody diluent and incubated overnight at 4°C. After washing with PBS, slides were incubated with goat anti-rabbit IgG highly cross-adsorbed-Alexa594 (Thermo Fisher Scientific, A-11037) and goat anti-mouse IgG highly cross-adsorbed Alexa647 (Thermo Fisher Scientific, A-21236) were diluted at 1:1000 in the antibody diluent and incubated for 2 hours at room temperature. The slides were washed with PBS, mounted using Vectashield with DAPI (Vector Labs, H-1200) and imaged with a Zeiss LSM 880 confocal microscope (Stanford Microscopy Facility). Colocalization of RIG-I and K63-polyUb were counted if foci were directly overlapping with FITC-circRNA and/or each other.

Anti-RIG-I rabbit polyclonal primary antibody (Cell Signaling Technology, 3743S) and anti-YTHDF2 mouse polyclonal antibody (USBiological, 135486) were diluted at 1:200 each in antibody diluent. The rest of the immunofluorescence including secondary staining, mounting, and imaging were done as detailed above. Colocalization of RIG-I and YTHDF2 were counted if foci were directly overlapping with FITC-circRNA and/or each other.

IRF3 dimerization assay

This assay was performed as described previously (Ahmad et al., 2018). Briefly, HEK293T cells were homogenized in hypotonic buffer (10 mM Tris pH 7.5, 10 mM KCl, 0.5 mM EGTA, 1.5 mM MgCl$_2$, 1 mM sodium orthovanadate, 1X mammalian Protease Arrest (GBiosciences, 786-108)) and centrifuged at 1000 g for 5 minutes to pellet the nuclei. The supernatant (S1), containing the cytosolic and the mitochondrial fractions, was used for *in vitro* IRF3 dimerization assay. The stimulation mix containing 10 ng/µl RIG-I, 2.5 ng/µl K63-Ub$_n$ along with the indicated amounts of RNA was pre-incubated at 4°C for 30 minutes in (20 mM HEPES pH 7.4, 4 mM MgCl$_2$ and 2 mM ATP). ^{35}S-IRF3 was prepared by *in vitro* translation using TnT T7 Coupled Reticulocyte Lysate System (Promega, L4610) according to manufacturer's instructions. The IRF3 activation reaction was initiated by adding 1.5 µL of pre-incubated stimulation mix to 15 µL reaction containing 10 µg/µl of S1, 0.5 µL ^{35}S-IRF3 in (20 mM HEPES pH 7.4, 4 mM MgCl$_2$ and 2 mM ATP) and incubated at 30°C for 1 hour. Subsequently, the samples were centrifuged at 18,000 g for 5 minutes and the supernatant was subjected to native PAGE analysis. IRF3 dimerization was visualized by autoradiography and phosphorimaging (Fuji, FLA9000).

Statistical Analyses

All statistical analysis was done with the software Graphpad Prism (GraphPad Software, La Jolla, CA). Student's t-, Kruskal-Wallis, or Anova-Tukey test was used whenever appropriate. *p* values less than 0.05 were considered statistically significant.

DATA AND CODE AVAILABILITY

The accession number for the m^{6}A-irCLIP sequencing data reported in this paper is deposited in Gene Expression Omnibus: GEO: GSE116007.